iScience

CellPress
OPEN ACCESS

Article

Single-cell RNA sequencing identifies a migratory keratinocyte subpopulation expressing THBS1 in epidermal wound healing

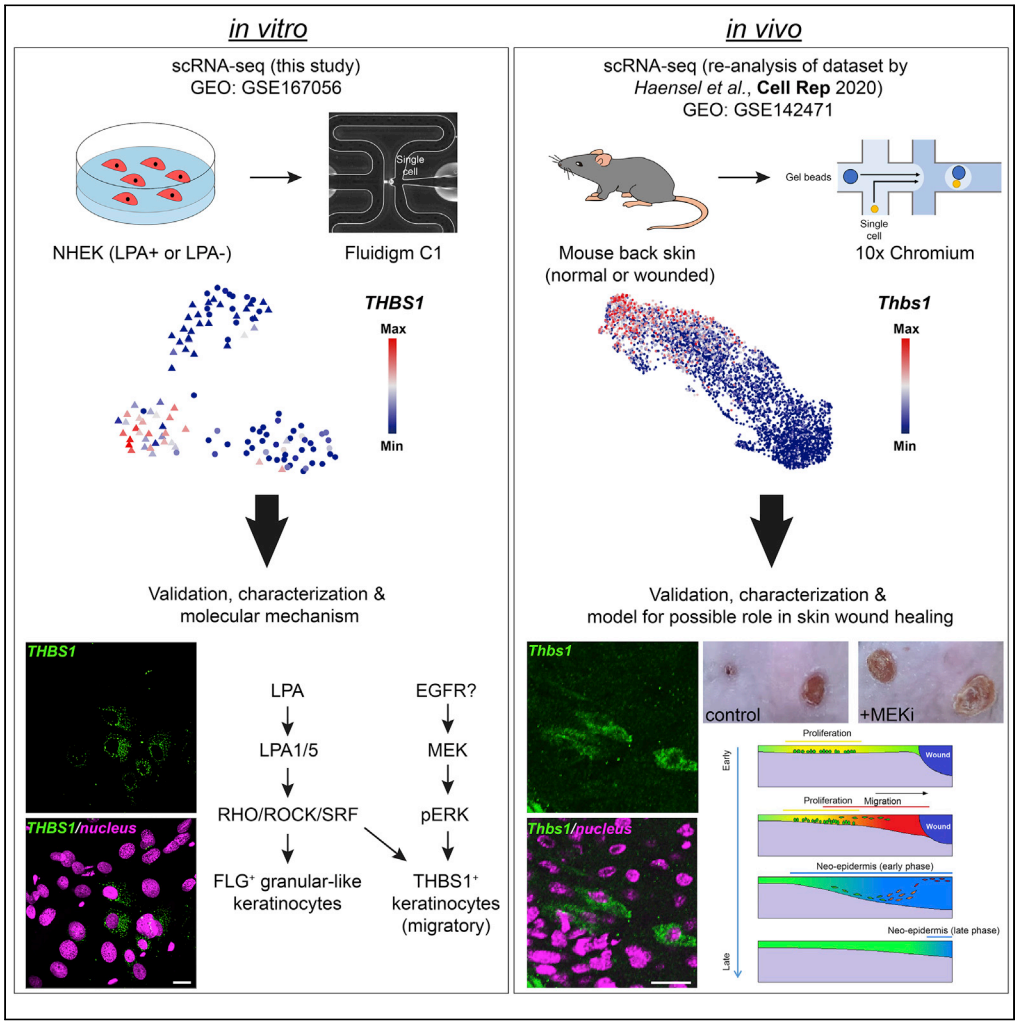

Ratklao Siriwach, Anh Quynh Ngo, Makio Higuchi, ..., Akira Watanabe, Shuh Narumiya, Dean Thumkeo

snaru@mfour.med.kyoto-u.ac.jp (S.N.)
d.thumkeo@mfour.med.kyoto-u.ac.jp (D.T.)

Highlights

Single-cell RNA sequencing reveals a keratinocyte subpopulation expressing THBS1

LPA and ERK activity are required for the induction of THBS1^{+} keratinocyte

Thbs1^{+} keratinocytes are differentiated from basal keratinocytes upon epidermal wounding

Thbs1^{+} keratinocytes are migratory cells and may contribute to epidermal wound healing

Siriwach et al., iScience 25, 104130
April 15, 2022
https://doi.org/10.1016/j.isci.2022.104130

iScience

CellPress
OPEN ACCESS

Article

Single-cell RNA sequencing identifies a migratory keratinocyte subpopulation expressing THBS1 in epidermal wound healing

Ratklao Siriwach,[1,3] Anh Quynh Ngo,[1,3] Makio Higuchi,[1] Kentaro Arima,[1] Satoko Sakamoto,[2] Akira Watanabe,[2] Shuh Narumiya,[1,*] and Dean Thumkeo[1,4,*]

SUMMARY

Keratinocyte differentiation is an intricate process that is regulated by multiple mediators. Using cultured human keratinocytes, we found that lysophosphatidic acid (LPA) induced the differentiation of a previously unsuspected keratinocyte subpopulation expressing the extracellular matrix protein, thrombospondin-1 (THBS1). This action of LPA was mediated by the RHO/ROCK-SRF signaling downstream of LPA_1 and LPA_5 receptors and required ERK activity. Suppression of THBS1 *in vitro* suggested a migratory role of $THBS1^+$ keratinocytes. Moreover, we analyzed publicly deposited single-cell RNA sequencing dataset and identified *Thbs1*-expressing keratinocytes in the mouse wound skin. Immunohistochemistry analysis revealed that $Thbs1^+$ keratinocytes were apparently differentiated from basal keratinocytes upon wounding, subsequently polarized and migrated suprabasally toward the wound front, and eventually underwent terminal differentiation in the neo-epidermis. Importantly, inhibition of Erk activity suppressed $Thbs1^+$ keratinocyte differentiation in wound healing. Based on these findings, we suggest that $THBS1^+$ keratinocyte is a migratory keratinocyte subpopulation that facilitates epidermal wound healing.

INTRODUCTION

The epidermis of human skin functions as a barrier and protects our body against dehydration, physical damage, external antigen exposure, and pathogen invasion (Elias, 2007). As the predominant cell type in the epidermis, keratinocytes represent approximately 95 percent of the total epidermal cells (McGrath et al., 2004). They are conventionally classified into three different subpopulations namely the basal, spinous, and granular keratinocytes that reside in their corresponding layers of the epidermis and are covered by the outermost *stratum corneum* (McGrath et al., 2004). In homeostasis, basal keratinocytes proliferate and subsequently differentiate into spinous and then granular keratinocytes, and the balance of this differentiation process is regulated by multiple growth factors and bioactive mediators (An et al., 1998; Kim et al., 2004).

Lysophosphatidic acid (LPA) is a lipid mediator of the lysophospholipid family and multiple species of LPA have been detected *in vivo* (Aoki et al., 2008; Aikawa et al., 2015). It is produced either from lysophospholipids by the action of lysophospholipase D/autotaxin in the serum or from phosphatidic acid by phospholipase A1 or A2 on the cell membrane (Aoki et al., 2008). In the skin, it is known that LPA could be synthesized through the catalytic activity of the enzyme mPA-$PLA_1\alpha$ (or LIPH) that is expressed in epidermal keratinocytes (Aoki et al., 2008; Diribarne et al., 2012). As a bioactive mediator, LPA is involved in various cellular processes such as cell proliferation, anti-apoptosis, migration, cytokine and chemokine secretion, platelet aggregation, contraction and transformation of smooth muscles, and neurite retraction (Aikawa et al., 2015). It is known that LPA exerts its physiological functions through six cognate G protein-coupled receptors (GPCRs), $LPA_{1\text{-}6}$ (Aikawa et al., 2015; Yung et al., 2015). In the skin, it was previously reported that LPA regulates hair follicle development through LPA_6 (Shimomura et al., 2008; Pasternack et al., 2008; Inoue et al., 2011). Moreover, we have recently reported that LPA facilitates the differentiation of basal keratinocytes to granular keratinocytes through the RHO/ROCK-SRF signaling downstream of LPA_1 and LPA_5, and this action of LPA enhances skin barrier function *in vivo* (Sumitomo

[1]Department of Drug Discovery Medicine, Kyoto University Graduate School of Medicine, Kyoto 606-8507, Japan

[2]Medical Innovation Center, Kyoto University Graduate School of Medicine, Kyoto 606-8507, Japan

[3]These authors contributed equally

[4]Lead contact

*Correspondence: snaru@mfour.med.kyoto-u.ac.jp (S.N.), d.thumkeo@mfour.med.kyoto-u.ac.jp (D.T.)

https://doi.org/10.1016/j.isci.2022.104130

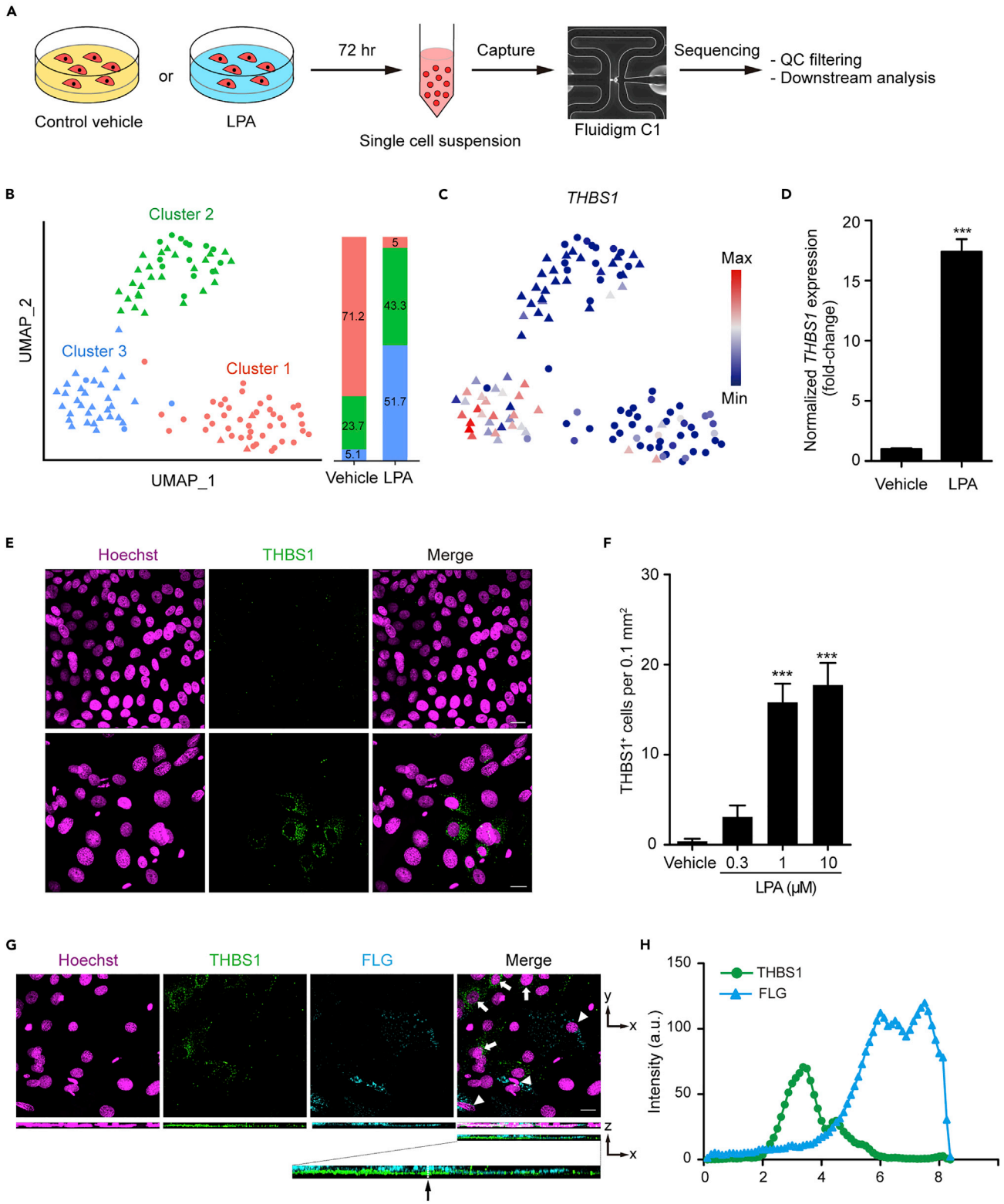

Figure 1. LPA induced THBS1^{+} keratinocytes *in vitro*

(A) Overview of the workflow for scRNA-seq analysis of NHEKs.

(B) Two-dimensional visualized with uniform manifold approximation and projection (UMAP) of cells that passed the quality control (n = 119), colored according to unsupervised clustering. Round mark (◯) indicates control NHEKs and triangle mark (△) indicates cells treated with 10 μM LPA for 72 h. Bar chart on the right indicates the percentage of cells assigned to each cluster per condition, colored according to unsupervised clustering.

Figure 1. *Continued*

(C) Feature plot showing *Thrombospondin-1* (*THBS1*) expression projected on UMAP.

(D) LPA (10 μM) induced *THBS1* gene expression as quantitated by qRT-PCR. Normalized fold changes are shown using *GAPDH* as the reference. Results are represented as means ± SEM, n = 3 for each condition. ***p < 0.001 (two-tailed Student's *t* test).

(E) Representative stacked confocal images of immunofluorescence staining of nuclei (Hoechst 33342, magenta) and THBS1 (green) in NHEKs treated with vehicle or 10 μM LPA for 72 h. Scale bars, 20 μm.

(F) Quantification of THBS1$^+$ cell number per area of 0.1 mm^2 induced by different LPA concentrations. Positive cells were counted over 10 representative pictures per condition (duplicates) and results are shown as means ± SEM, ***p < 0.001 (Kruskal-Wallis test followed by Dunn's multiple comparisons test).

(G) Representative stacked confocal images of immunofluorescence staining of nuclei (Hoechst 33342, magenta), THBS1 (green), and the granular keratinocyte marker, FLG (cyan) of NHEKs stimulated with 10 μM LPA for 72 h. Reconstituted image on the x-z axis is shown below. Note the different spatial location of THBS1$^+$ keratinocytes (white arrows) in the bottom cell layer and FLG$^+$ keratinocytes (white arrowheads) in the upper cell layers. Scale bar, 20 μm.

(H) Linescan profiles of the signal intensities of THBS1 and FLG along the dotted white line shown in the corresponding images in (G).

et al., 2019). However, given the pleiotropic activity of LPA in different physiological and developmental processes, unsuspected roles of LPA in the skin remain to be explored.

Skin wound healing is a highly dynamic process in which different cell types work together in a coordinated fashion under the tight control of various wound-induced mediators (Cañedo-Dorantes and Cañedo-Ayala, 2019). LPA is one such mediator that was detected at relatively high concentrations in blister fluids of injured skin (Mazereeuw-Hautier et al., 2005) and has been shown to promote wound healing (Demoyer et al., 2000; Balazs et al., 2001). Previous works have proposed that LPA facilitates wound healing through various different mechanisms such as debris clearance via macrophage accumulation and wound contraction via increased contractility of fibroblasts and collagen matrix (Mio et al., 2002; Zhao et al., 2005; Abe et al., 2007). However, how LPA directly modulates keratinocyte functions in the wound healing process remains largely unknown and needs further investigation.

Single-cell RNA sequencing (scRNA-seq) is a novel and powerful technology that allows the detection and quantification of gene expression at single-cell resolution (Kolodziejczyk et al., 2015). Since its first introduction in 2009 (Tang et al., 2009), with subsequent technology breakthroughs and reducing cost, scRNA-seq has been rapidly introduced into various fields of biology and medicine. By enabling the transcriptomic profiling of thousands of cells in parallel, scRNA-seq not only uncovers the uniqueness of each cell within a population but also helps researchers to address various biological questions regarding new cell types/phenotypes, cellular state transition, developmental dynamics, gene regulatory networks, and allele-specific gene expression (Grün et al., 2015; Rizvi et al., 2017; Xue et al., 2013; Benitez et al., 2017). In the field of skin biology, several scRNA-seq studies on mouse and human skin have been recently reported (Joost et al., 2016, 2018, 2020; Cheng et al., 2018; Finnegan et al., 2019; Haensel et al., 2020; Reynolds et al., 2021). These studies have revealed the marked heterogeneity of keratinocytes in skin both in homeostasis and under pathophysiological conditions. In this study, we employed scRNA-seq to further unravel LPA actions on keratinocyte differentiation and its previously unsuspected roles in epidermal wound healing.

RESULTS

LPA induced a novel THBS1$^+$ keratinocyte subpopulation *in vitro*

We previously reported that LPA facilitates the differentiation of granular keratinocytes using normal human epidermal keratinocytes (NHEKs) isolated from neonatal foreskin (Sumitomo et al., 2019). However, in our previous study, besides FLG$^+$ granular keratinocytes, a fraction of keratinocytes was stained negative for FLG under LPA stimulation. Moreover, the morphology of these keratinocytes was distinct from undifferentiated NHEKs in the control condition. Based on these observations, we hypothesized that LPA might also induce a subpopulation of keratinocytes that is different from the control NHEKs and granular keratinocytes. To test this hypothesis, we employed scRNA-seq to dissect the transcription profiles of NHEKs stimulated with either vehicle or 10 μM LPA for 72 h at single-cell resolution (Figure 1A). After quality control (Figures S1A–S1G), 59 cells from the control group and 60 cells from the LPA treatment group were subjected for downstream analysis. Unsupervised clustering of integrated scRNA-seq data (n = 119) using graph-based clustering in Seurat (Gribov et al., 2010) identified three different subpopulations of keratinocytes (Figure 1B, left). It should also be noted that most of vehicle-treated control cells were classified in cluster 1 keratinocytes, whereas the majority of LPA-treated cells were classified in cluster 2 and 3 keratinocytes (Figure 1B, right). We further conducted differential expression genes (DEGs) analysis on each cluster to identify the specific marker genes for each cluster (Table S1). We found

that cluster 1 keratinocytes expressed the highest levels of basal keratinocyte markers, *KRT5* and *KRT14*, among the 3 clusters, and therefore annotated them as basal-like keratinocytes (Figure S2A). On the other hand, given its high expression of early granular keratinocyte markers such as *TGM1* and *SCEL* and partial expression of late granular keratinocyte markers such as *IVL* and *FLG*, cluster 2 was annotated as granular-like keratinocytes (Figure S2A). Interestingly, we found that cluster 3 keratinocytes significantly expressed high levels of *thrombospondin-1* (*THBS1*), a matricellular protein involved in tissue repair (Tan and Lawler, 2009; Adams and Lawler, 2011; Sweetwyne and Murphy-Ullrich, 2012; Resovi et al., 2014) and therefore, annotated cluster 3 as *THBS1*-expressing keratinocytes (Figures 1C and S2B). Gene set enrichment analysis (GSEA) further indicated a number of gene sets significantly enriched in *THBS1*-expressing keratinocytes compared to the basal keratinocytes, especially those involved in cell migration such as actomyosin, anchoring, and cell-substrate junction (Figure S2C and Table S2). Moreover, we generated violin plots for genes listed in GO term "EMT (epithelial-mesenchymal transition)" and found that some of representative EMT genes such as *HMGA2*, *FLNA*, *TGFBR1*, and *NOTCH1* were highly expressed in cluster 3 (Figure S2D). Given these results, we deduced that LPA promotes the differentiation of NHEKs to two cell populations, granular-like keratinocytes and a unique subpopulation of keratinocytes specifically expressing *THBS1* with enriched migratory signatures.

To validate the LPA-induced *THBS1*-expressing keratinocytes as suggested by scRNA-seq analysis, we next examined *THBS1* gene expression by quantitative RT-PCR (qRT-PCR) and confirmed that LPA significantly enhanced *THBS1* expression (Figure 1D). Moreover, we examined the presence of *THBS1*-expressing keratinocytes by immunocytochemistry for THBS1. Although THBS1 was rarely detected in vehicle-treated control NHEKs, it was clearly observed in the perinuclear region of a fraction of cells treated with LPA (Figure 1E). Given that the perinuclear staining of THBS1 in ER and Golgi apparatus is consistent with THBS1 staining pattern observed in other cell types (Cunha et al., 2016; Jerónimo et al., 2017), we defined keratinocytes detected with such perinuclear THBS1 signals as $THBS1^+$ keratinocytes. We found an increased number of $THBS1^+$ keratinocytes in an LPA concentration-dependent manner, whereas they were rarely detected among vehicle-treated control NHEKs (Figure 1F). Notably, $THBS1^+$ keratinocytes in LPA-treated NHEKs tended to form small clusters consisting of several cells (Figure 1E). Co-staining with a different anti-THBS1 antibody showed a complete overlap of perinuclear signals, further supporting that these signals specifically represent THBS1 (Figures S3A and S3B).

In addition, co-immunostaining for THBS1 and FLG revealed that LPA-induced $THBS1^+$ cells were distinct from FLG^+ granular keratinocytes (Figure 1G). They were always mutually exclusive. Notably, there was a remarkable difference in the three-dimensional spatial localization between these two subpopulations in differentiated-multilayered NHEKs such that $THBS1^+$ keratinocytes were mainly located at the bottom, whereas FLG^+ keratinocytes were localized on the top layers (Figure 1H). Taken together, these results indicate that LPA induced $THBS1^+$ keratinocytes in addition to FLG^+ granular keratinocytes *in vitro*.

Characterization of $THBS1^+$ keratinocyte subpopulation induced by LPA

We next conducted immunocytochemistry to further examine the characteristics of $THBS1^+$ keratinocytes induced by LPA. First, we treated NHEKs with vehicle or 10 μM LPA for 72 h and conducted co-staining of THBS1 and Ki67, a cell proliferation marker. Both $THBS1^+Ki67^+$ keratinocytes and $THBS1^+Ki67^-$ keratinocytes could be observed upon LPA treatment (Figure 2A), suggesting that $THBS1^+$ keratinocytes were composed of both proliferative cells and cells that exit the cell cycle at this time point. It should be noted that LPA did not trigger apoptosis in NHEKs as TUNEL staining showed no significant difference between vehicle control and LPA-treated conditions (Figures 2B and 2C). Therefore, LPA induced $THBS1^+$ keratinocytes without affecting cell apoptosis.

We next conducted small interfering RNAs (siRNAs)-mediated knockdown experiments to investigate the function of THBS1 produced by $THBS1^+$ keratinocytes (Figure 2D). Given the involvement of THBS1 in wound healing previously reported in literature (DiPietro et al., 1996; Agah et al., 2002; Nor et al., 2005), we examined the wound-healing capability of keratinocytes upon *THBS1* knockdown using an *in vitro* scratching assay. Time-lapse imaging revealed that knockdown of *THBS1* resulted in slower wound healing compared to the control (Figure 2E and Video S1). Quantification of the reepithelialized area versus time further revealed a significant delay in cell migration upon *THBS1* knockdown (Figure 2F). These results suggest a critical role of THBS1 produced by $THBS1^+$ keratinocytes in epidermal wound healing.

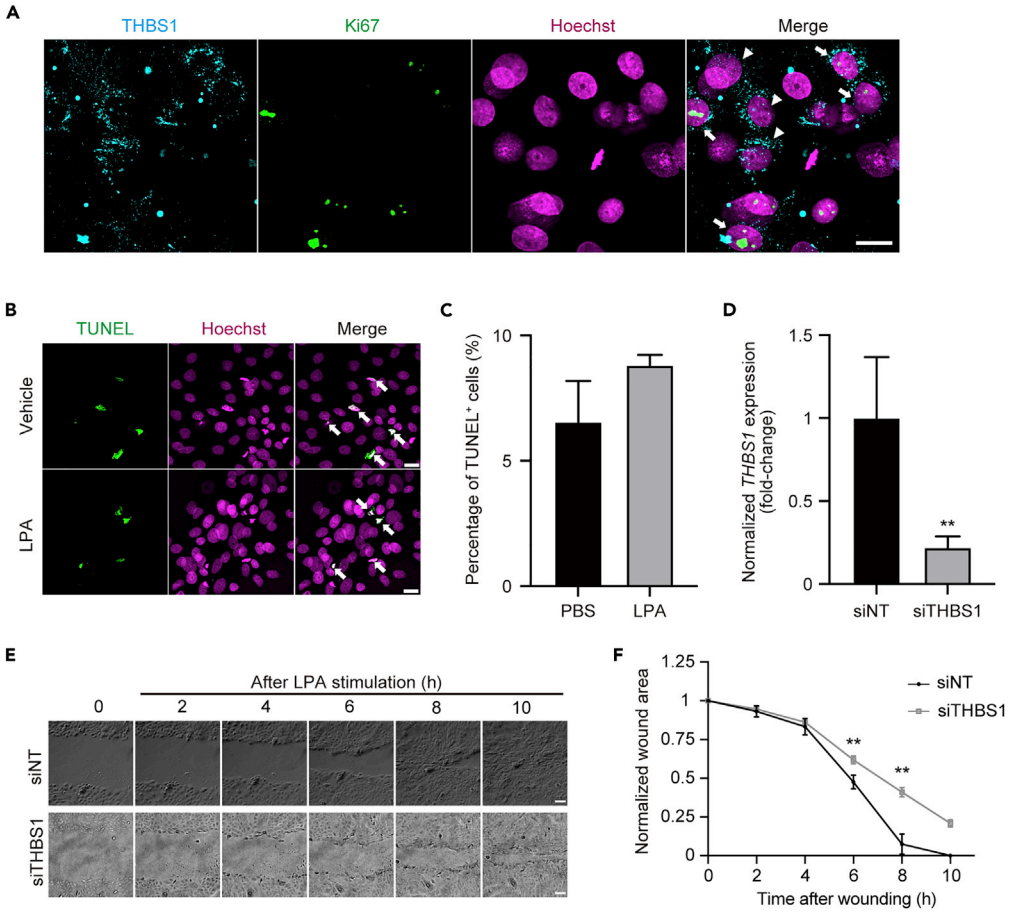

Figure 2. Characterization of *in vitro* LPA-induced THBS1$^+$ keratinocytes

(A) Representative stacked confocal images of immunofluorescence staining of THBS1 (cyan), Ki67 (green), and nuclei (Hoechst 33342, magenta) in NHEKs stimulated with 10 μM LPA for 72 h. White arrows indicate THBS1$^+$Ki67$^+$ keratinocytes and white arrowheads indicate THBS1$^+$Ki67$^-$ keratinocytes. Scale bar, 20 μm.

(B) Representative stacked confocal images of immunofluorescence staining of TUNEL (green), and nuclei (Hoechst 33342, magenta) in NHEKs treated with vehicle or 10 μM LPA for 72 h. White arrows indicate TUNEL$^+$ keratinocytes. Scale bars, 20 μm.

(C) Quantification of the percentage of TUNEL$^+$ keratinocytes per total keratinocytes induced by 10 μM LPA for 72 h. Positive cells were counted over 10 representative pictures per condition (triplicates) and results are shown as means ± SEM. There was no statistical significance between the two conditions (two-tailed Student's *t* test).

(D) siRNA-mediated knockdown of *THBS1* in NHEKs. Suppression of *THBS1* gene expression at the time of stimulation (24 h after siRNA transfection) is shown. Normalized fold changes are shown using *GAPDH* as the reference. Results are represented as means ± SEM, n = 3 for each condition. **p < 0.01 (two-tailed Student's *t* test).

(E) Representative phase contrast images of control and *THBS1*-knockdown NHEKs after wound scratching every 2 h. Time is relative to wound scratching. Scale bars, 50 μm.

(F) Normalized wound area (wound area at each time point normalized to wound area at 0 h) as imaged in (E) is plotted versus time. Data is shown as means ± SD, n = 3 for each condition. **p < 0.01 (two-tailed Student's *t* test at each time point).

THBS1$^+$ keratinocyte induction was regulated by Rho/ROCK-SRF signaling downstream of LPA$_1$ and LPA$_5$ receptors

We previously reported that LPA promotes NHEK differentiation to FLG$^+$ granular keratinocytes via LPA$_1$ and LPA$_5$ receptors (Sumitomo et al., 2019). Given these findings, we next examined the involvement of LPA$_1$ and LPA$_5$ receptors in THBS1$^+$ keratinocyte differentiation with siRNAs. We selectively knocked down the expression of *LPAR1*, *LPAR5*, or both in NHEKs. siRNA for each receptor was confirmed to effectively knockdown the respective receptor (Figures 3A and 3B). Single knockdown of *LPAR1* suppressed LPA-induced *THBS1* expression by ~60%, single knockdown of *LPAR5* by ~15%, and combined

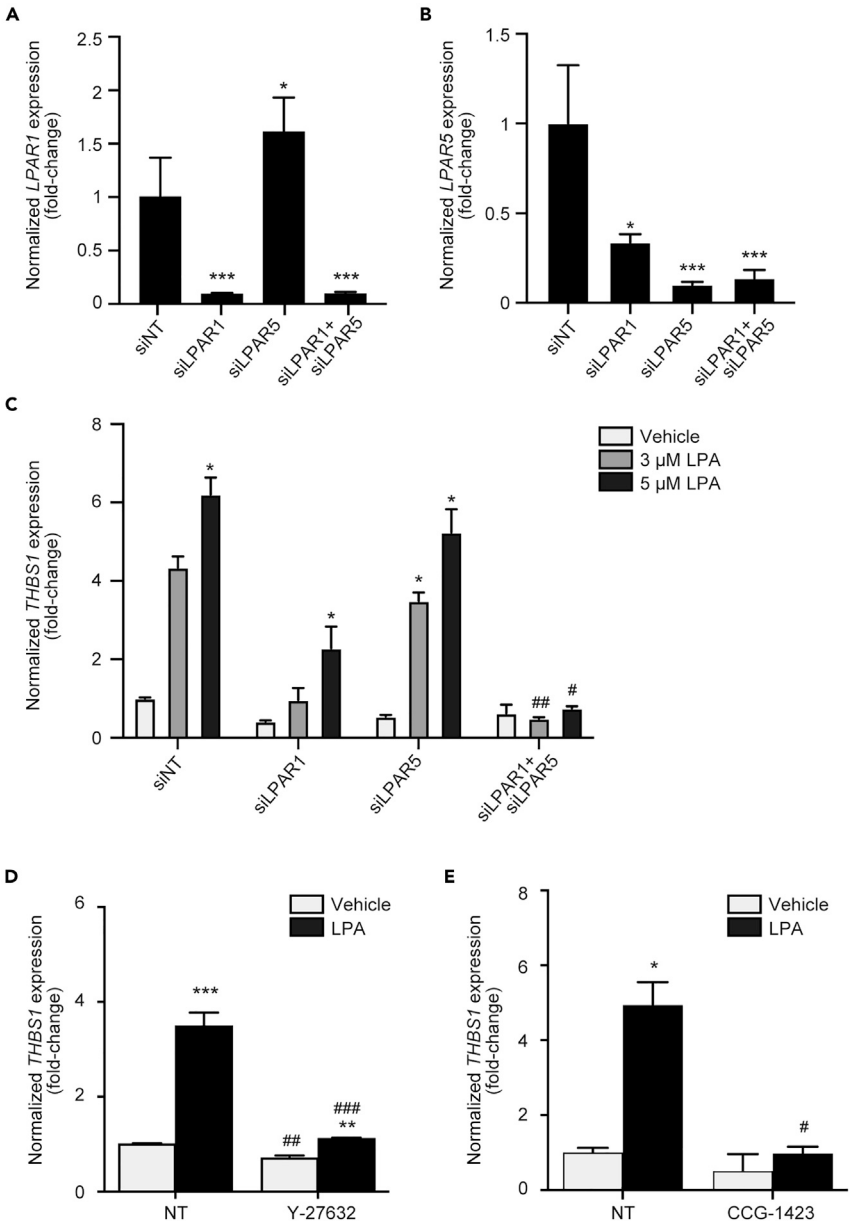

Figure 3. LPA induced THBS1^{+} keratinocytes through Rho/ROCK-SRF signaling downstream of LPA$_1$/LPA$_5$ receptors

(A and B) siRNA-mediated single and double knockdown of *LPAR1* and *LPAR5* in NHEKs. *LPAR1* and *LPAR5* gene expressions were measured by qRT-PCR at the time of LPA stimulation (24 h after siRNA transfection). Normalized fold changes are shown using *GAPDH* as the reference. Results are represented as means ± SEM, n = 3 for each condition. *p < 0.05, ***p < 0.001 (compared with the control siNT group) (one-way ANOVA followed by Bonferroni's post-hoc comparisons test).

(C) *THBS1* gene expression in *LPAR1*-knockdown, *LPAR5*-knockdown, or *LPAR1/5*-double knockdown NHEKs upon LPA stimulation for 72 h. Normalized fold changes are shown using *GAPDH* as the reference. Results are represented as means ± SEM, n = 3 for each condition. *p < 0.05 (compared with the vehicle control of the indicated treated group) (Kruskal-Wallis test followed by Dunn's multiple comparisons test), $^{\#}$p < 0.05, $^{\#\#}$p < 0.01 (compared with the siNT control of the corresponding LPA stimulation) (Kruskal-Wallis test followed by Dunn's multiple comparisons test).

(D) 10 μM LPA-treated NHEKs in the absence or presence of Y-27632 (30 μM). LPA-induced *THBS1* gene expression at 72 h post-stimulation is shown.

Figure 3. *Continued*

(E) 10 μM LPA-treated NHEKs in the absence or presence of CCG-1423 (3 μM). LPA-induced *THBS1* gene expression at 72 h post-stimulation is shown. Results in (D) and (E) are shown in normalized fold changes with *GAPDH* as the reference and as means ± SEM, n = 3 for each condition. *$p < 0.05$, **$p < 0.01$, ***$p < 0.001$ (compared with the vehicle control of the indicated treated group) (two-tailed Student's *t* test), $^{\#}p < 0.05$, $^{\#\#}p < 0.01$, $^{\#\#\#}p < 0.001$ (compared with the control of the corresponding LPA stimulation) (one-way ANOVA followed by Bonferroni's post-hoc comparisons test).

knockdown of *LPAR1* and *LPAR5* additively suppressed LPA-induced *THBS1* expression by ~90% (Figure 3C). In addition, we conducted experiments using LPA_1 antagonist (AM095) or LPA_5 antagonist (TCLPA54) to further validate and consistently found a significant decrease in the number of $THBS1^+$ cells in the presence of either antagonist (Figures S4A and S4B). Therefore, LPA induces $THBS1^+$ keratinocytes through both LPA_1 and LPA_5 receptors. Given that we also previously reported that RHO/ROCK-SRF is the critical signaling pathway downstream of LPA_1 and LPA_5 for FLG^+ granular keratinocyte differentiation (Sumitomo et al., 2019), we next examined the role of this signaling pathway with a ROCK-specific inhibitor, Y-27632 (Uehata et al., 1997), and an SRF-specific inhibitor, CCG-1423 (Hayashi et al., 2014). We found that LPA-dependent *THBS1* expression was significantly suppressed in the presence of Y-27632 (Figures 3D and S4C) and CCG-1423 (Figure 3E). Taken together, these data suggest that similar to FLG^+ granular keratinocytes, LPA also induced $THBS1^+$ keratinocytes via LPA_1 and LPA_5 receptors and their downstream RHO/ROCK-SRF signaling.

ERK activity dictates the different cell fates of NHEKs upon LPA stimulation

Given that LPA induced both $THBS1^+$ keratinocytes and FLG^+ granular keratinocytes through the same LPA_1/LPA_5-RHO/ROCK-SRF signaling, we next questioned what determines the different cell fates of NHEKs. We reasoned that cellular heterogeneity of NHEKs at the time of LPA stimulation might be the underlying critical factor responsible for such cell fate decisions. Given that the heterogeneity of ERK activity in cultured cells including keratinocytes was previously reported (Aoki et al., 2013; Hiratsuka et al., 2015, 2020), we examined ERK activity in our cultured NHEKs by immunocytochemistry for phosphorylated ERK (pERK). We found that there were two different types of staining patterns of pERK in NHEKs: nuclear staining and diffused staining patterns (Figure 4A). Notably, nuclei of NHEKs that showed diffused-pERK staining pattern were located slightly higher from the bottom cell layer (Figure 4A, below) than nuclei of NHEKs with nuclear-pERK staining pattern (Figure 4A, below). Moreover, the staining intensity was varied among NHEKs with nuclear-pERK staining pattern (Figure 4B). Double staining of pERK and Ki67 further revealed a positive correlation between nuclear-pERK staining and Ki67 staining (Figures S5A and S5B). These results together suggest that there is a large heterogeneity of ERK activity in cultured NHEKs before LPA stimulation, and cells with high ERK activity are proliferative cells.

We next examined how ERK activity affects NHEK differentiation upon LPA stimulation. To this end, we used U0126, a MEK-specific inhibitor. MEK is an upstream kinase of ERK and it was previously reported that U0126 binds to the MEK1/2 kinases and inhibits their phosphorylation and subsequent ERK activation (Cargnello and Roux, 2011). First of all, we confirmed that U0126 treatment for 30 min significantly suppressed nuclear ERK staining (Figures S6A and S6B). We then next pre-treated NHEKs with U0126 for 30 min to suppress ERK activity, stimulated with LPA for 72 h, and then examined the number of $THBS1^+$ and FLG^+ keratinocytes. We found that the number of FLG^+ keratinocytes was increased in the presence of U0126 (Figures 4C and 4D). This result was consistent with our previous report (Sumitomo et al., 2019). In contrast, the number of $THBS1^+$ keratinocytes upon LPA treatment for 72 h was significantly reduced in the presence of U0126 (Figures 4C and 4E). It should be noted that treatment of NHEKs with U0126 without LPA stimulation had no significant effect on the differentiation of both FLG^+ keratinocytes and $THBS1^+$ keratinocytes (Figures 4D and 4E). These results suggest that ERK activity at the moment of LPA stimulation is indispensable for the induction of $THBS1^+$ keratinocytes but not FLG^+ keratinocytes.

To determine possible sources of basal ERK activity, we further investigated the involvement of EGFR, a receptor for the growth factor EGF, in $THBS1^+$ keratinocyte induction. It is widely known that MEK-ERK signaling cascade is activated downstream of EGFR (Lemmon and Schlessinger, 2010). We used PD168393, an EGFR-specific inhibitor, and found that the number of $THBS1^+$ keratinocytes, but not FLG^+ keratinocytes, upon LPA treatment was reduced in the presence of EGFR inhibitor (Figures S7A and S7B) in a similar fashion to MEK inhibitor (Figures 4C–4E). Therefore, it is likely that signaling through

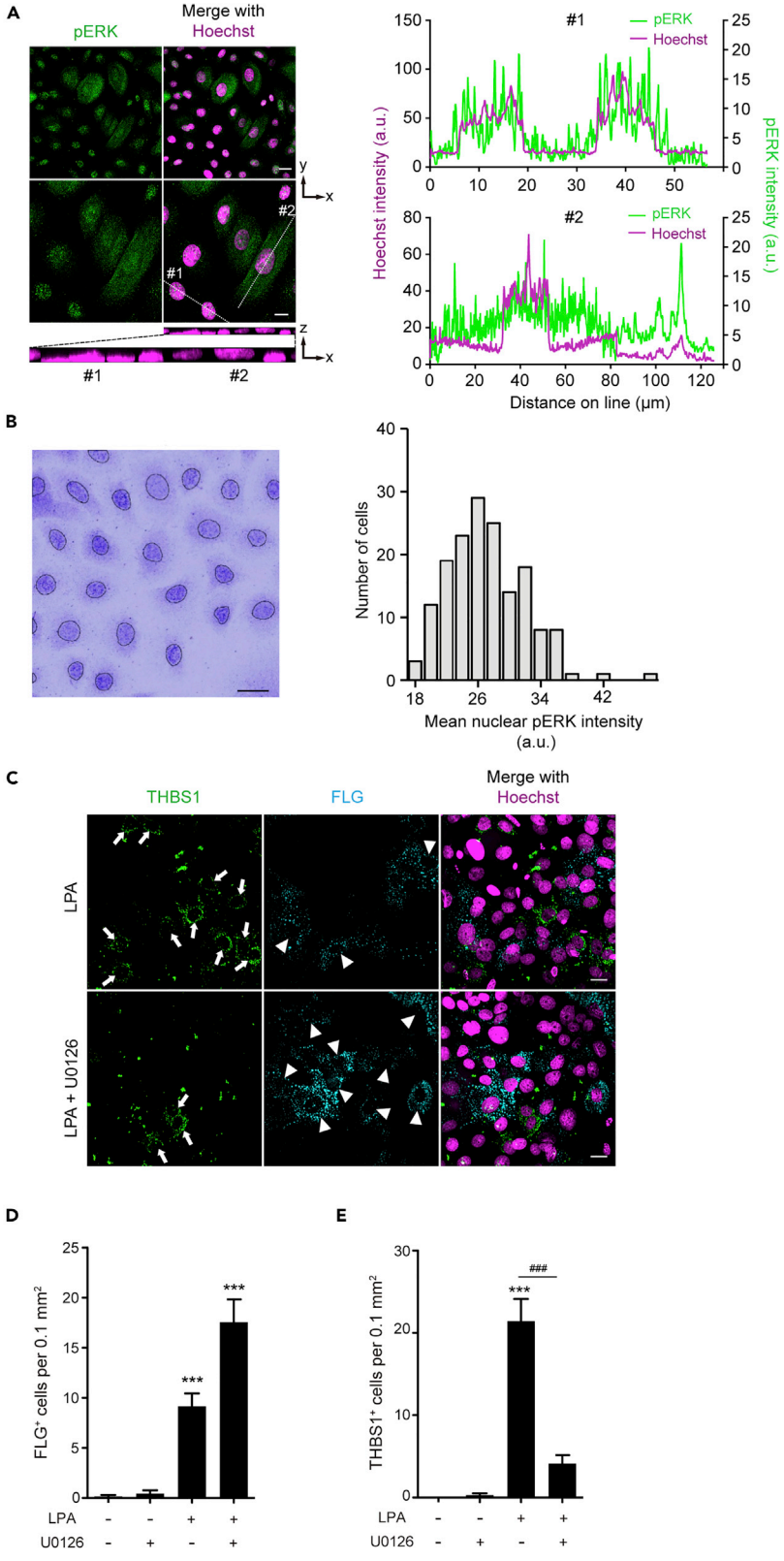
A
pERK
Merge with Hoechst
y
x
#2
#1
z
x
#1
#2
#1
pERK
Hoechst
#2
pERK
Hoechst
Hoechst intensity (a.u.)
pERK intensity (a.u.)
Distance on line (μm)
B
Number of cells
Mean nuclear pERK intensity (a.u.)
C
THBS1
FLG
Merge with Hoechst
LPA
LPA + U0126
D
FLG+ cells per 0.1 mm2
***
***
LPA
U0126
E
THBS1+ cells per 0.1 mm2
***
###
LPA
U0126

Figure 4. Heterogeneity of basal ERK activity in NHEKs and the dependence of LPA-induced THBS1$^+$ keratinocytes

(A) Representative stacked confocal images of immunofluorescence staining of pERK (green) and pERK (green) merged with nuclei (Hoechst 33342, magenta) in unstimulated NHEKs at 0 h. Note different distributions of pERK in the nucleus or cytoplasm in different keratinocytes. Reconstituted image of nuclei on the x-z axis is shown below and enlarged. Note that nuclei of keratinocytes with diffused pERK staining patterns were located higher than nuclei of other keratinocytes. Scale bars, 20 μm. Linescan profiles of signal intensities of pERK and nuclei along the dotted white line shown for two cells (#1 = nuclei staining pattern & #2 = diffused staining pattern) are shown on the right side.

(B) Representative stacked confocal images of immunofluorescence staining of pERK in unstimulated NHEKs at 0 h that showed nuclear staining pattern. Image intensity was scaled to a normalized-pERK intensity and range from 0 to 100 a.u. (arbitrary units). Quantification of the mean nuclear-pERK staining intensity in NHEKs is shown on the right side (n = 162 cells).

(C–E) Representative stacked confocal images of NHEKs stimulated with 3 μM LPA for 72 h in the absence (C, upper) or presence of 5 μM U0126 (C, lower) and quantification of FLG$^+$ (D) and THBS1$^+$ (E) cell number per area of 0.1 mm^2. Scale bars, 20 μm. Positive cells were counted over 15 representative pictures per condition (triplicates) and results are shown as means ± SEM, ***$p < 0.001$ (compared with the vehicle control), $^{###}p < 0.001$ (other comparisons) (Kruskal-Wallis test followed by Dunn's multiple comparisons test).

EGFR regulates the ERK activity in NHEKs and contributes to THBS1$^+$ keratinocyte differentiation. It should be noted that we also examined the involvement of phosphatidylinositol three-kinase (PI3K) using a specific inhibitor, Wortmannin, and found that it stimulated both *FLG* and *THBS1* expression (Figures S7C and S7D), thus suggesting that PI3K plays an inhibitory role in the LPA-induced NHEK differentiation.

Thbs1$^+$ keratinocytes were specifically induced in the proliferation zone of epidermal basal layer upon wounding and subsequently migrated toward the wound front in mice

Given the previously reported elevation of *THBS1* expression in NHEKs upon scratching in *in vitro* wound assay (Fitsialos et al., 2007), our aforementioned findings that THBS1 promotes cell migration of NHEKs *in vitro*, and previous reports suggesting the upregulation of *Thbs1* in wounded skin of mice (Joost et al., 2018; Haensel et al., 2020), we speculated the involvement of THBS1$^+$ keratinocytes in epidermal wound healing. To examine this possibility, we investigated *Thbs1* expression in mouse interfollicular keratinocytes upon wound healing at day 4 post wound induction (PWI) using a public scRNA-seq dataset that was previously reported by Haensel et al., 2020. From this deposited data, we were able to reproduce the result of three basal keratinocyte states in the interfollicular epidermis (IFE): *Col17a1*-hi, ER (early response), and GA (growth arrest) (Figures 5A and 5B) as previously described (Haensel et al., 2020). In this work by Haensel et al., it was demonstrated that GA basal keratinocytes are specifically increased upon wounding and could be observed in the migrating front of the wound in the IFE (Haensel et al., 2020). Intriguingly, our reanalysis results further revealed that GA basal keratinocytes specifically expressed high *Thbs1* levels compared to the other IFE basal keratinocytes (Figure 5C). In addition, GO analysis indicated that GA basal keratinocytes possessed migratory signatures with significant enrichment for cell migration-related gene sets (Figure 5D). Based on these findings, we deduced a possibility that Thbs1$^+$ keratinocytes are differentiated from basal keratinocytes and acquire migratory ability upon epidermal wounding *in vivo*.

To further validate the presence of Thbs1$^+$ keratinocytes in wound skin, we conducted immunohistochemistry of Thbs1 at different time points in the dorsal skin of mice subjected to excisional dorsal full-thickness skin wounds (Figure 6A). The specificity of Thbs1 staining in the epidermis was confirmed by the use of two different antibodies that show an identical staining pattern (Figures S8A and S8B). In normal skin, Thbs1$^+$ keratinocytes were rarely observed in the IFE and mainly restricted to keratinocytes in hair follicle (HF) bulges (Figure 6B). This finding is consistent with previous *in situ* hybridization findings on mRNA expression of *Thbs1* (Streit et al., 2000). Intriguingly, wounded skin at day 1 PWI showed a large number of Thbs1$^+$ keratinocytes in the basal layer of the epidermis spanning a distance of 0.6–1 mm from the wound edge (Figures 6C and 6I), presumably in the proliferation zone as defined by previous studies (Aragona et al., 2017; Park et al., 2017). Consistently, double staining of Thbs1 together with Ki67 indicated a number of Thbs1$^+$ keratinocytes positive for Ki67 in the proliferation zone (Figure S9A). It should be noted that nuclei of Thbs1$^+$ keratinocytes were relatively round at this stage (Figure 6C). Co-staining of Thbs1 and Krt14 further revealed that Thbs1$^+$ keratinocytes are basal keratinocytes at day 1 PWI, because they are Krt14-positive (Figure S9B). Subsequently, on day 2 PWI, most of Thbs1$^+$ keratinocytes remained in the basal layer at approximately the same distance but with their nuclei elongated (Figures 6D and 6I). Notably, there were also some Thbs1$^+$ cells that detached from the basement membrane and were located in the

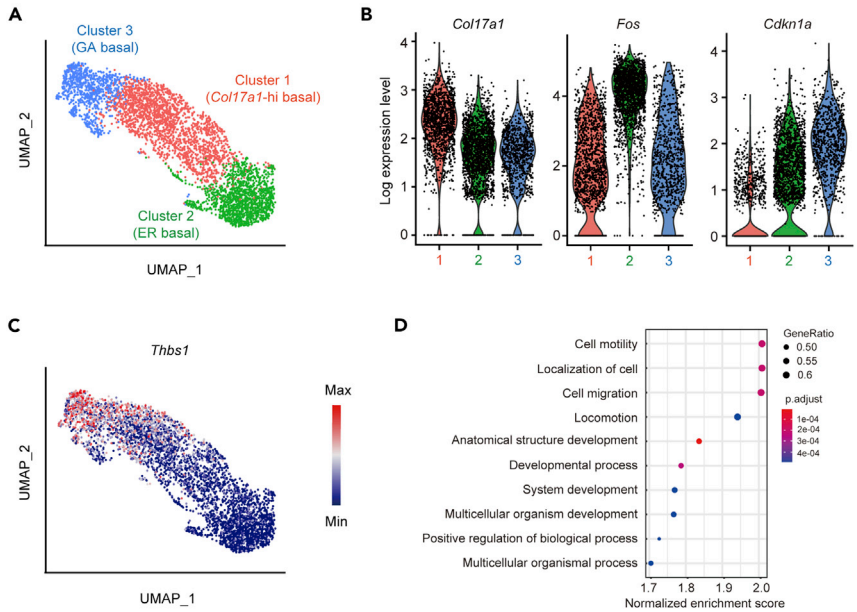

Figure 5. scRNA-seq analysis of interfollicular epidermis (IFE) basal keratinocytes in mice using publicly deposited data GEO: GSE142471

(A) Interfollicular epidermis (IFE) basal keratinocytes from both unwound and wound skin (n = 5 samples (2 unwound and three wound), total 4,099 cells) were visualized in two-dimension with UMAP and colored according to unsupervised clustering.

(B) Violin plots of representative marker genes (*Col17a1*, *Fos*, and *Cdkn1a*) for each basal cell state.

(C) Feature plot showing *Thbs1* expression projected on UMAP.

(D) Top 10 enriched GO terms of biological process in the cluster of GA basal keratinocytes versus the other 2 clusters. Gene ontology analysis was performed on differential expression genes ($p < 0.05$) using clusterProfiler (Yu et al., 2012; Wu et al., 2021) and GO gene sets. Enriched gene sets were ranked by normalized enrichment score, the size of the dot indicates the ratio of differentially expressed genes found in each gene set (GeneRatio), and the color represents the pathway enrichment significance (adjusted p value or p.adjust).

suprabasal layer (Figure 6D). We next observed an increased number of Thbs1$^+$ keratinocytes in the suprabasal layer at the distance closer to the wound edge (0.3–0.6 mm) at day 3 PWI (Figures 6E and 6I). This area is likely the migration zone as defined by previous studies (Aragona et al., 2017; Park et al., 2017). It should be noted that a fraction of Thbs1$^+$ keratinocytes at this stage was polarized, elongated, and apparently moved toward the wound front. These morphological characteristics are the hallmark of migratory cells. Moreover, polarized Thbs1$^+$ keratinocytes observed at day 4 PWI were Ki67-negative (Figure S9C). These results are consistent with the features of *T*hbs1-enriched GA keratinocytes at day 4 PWI described previously (Haensel et al., 2020), including migratory signatures and cell-cycle arrest.

On day 5 PWI when reepithelialization was completed, Thbs1$^+$ keratinocytes were found in the thick neo-epidermis (Figure 6F). Thbs1$^+$ keratinocytes formed a stream of cells that upwardly extended from the edge to the center of the neo-epidermis (Figure 6F). To examine the identity of these cells, Krt10, a spinous keratinocyte marker, was stained using consecutive skin sections. We found that the neo-epidermis consisted of multiple layers of Krt10$^+$ spinous keratinocytes but only a single layer of Krt10$^-$ basal keratinocytes. Notably, a fraction of Krt10$^+$ keratinocytes in lower suprabasal layers was also positive for Thbs1, suggesting Thbs1$^+$ keratinocytes further differentiated into spinous keratinocytes (Figure 6G). Finally, Thbs1 signals disappeared as the wound closure completed and the neo-epidermis became fully stratified on day 7 PWI (Figure 6H). Altogether, these findings suggest that Thbs1$^+$ keratinocytes differentiated into Krt10$^+$ spinous keratinocytes upon their arrival at the wound and then finally downregulated their Thbs1 expression.

Taken together, Thbs1$^+$ keratinocytes were apparently specifically generated from basal keratinocytes of the proliferation zone upon wounding, migrated toward the wound front, and eventually differentiated into spinous keratinocytes as they arrived at the neo-epidermis.

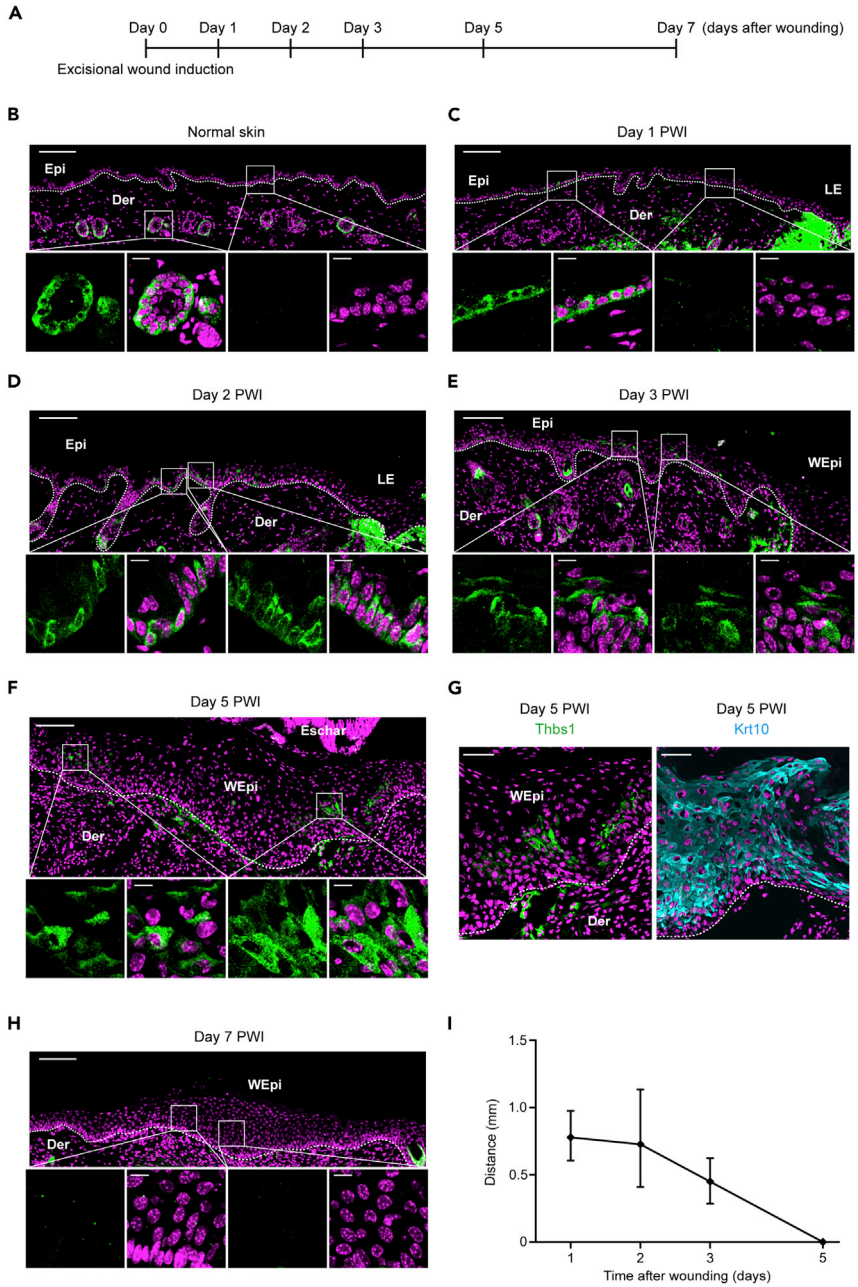

Figure 6. Thbs1^{+} keratinocytes were transiently induced upon wound healing *in vivo*

(A) Scheme represents the experiment design.

(B–F) Representative stacked confocal images showing immunostaining for Thbs1 (green) and nuclei (Hoechst 33342, magenta) in (B) normal skin and wounded skin on day 1, 2, 3, and 5 PWI (C–F). Dotted lines: approximate location of the basement membrane beneath the normal epidermis. Filled lines: approximate location of the basement membrane beneath the leading edge or neo-epidermis. Der, dermis; Epi, normal epidermis; Eschar, eschar; LE, leading edge; WEpi, neo-epidermis. Scale bars, 100 μm (low magnification), and 10 μm (high magnification).

(G) Representative stacked confocal images showing immunostaining for nuclei (Hoechst 33342, magenta), Krt10 (cyan blue), and Thbs1 (green) using consecutive wounded skin sections on day 5 PWI. Dotted lines: approximate location of the basement membrane beneath the neo-epidermis. Scale bars, 50 μm.

(H) Representative stacked confocal images showing immunostaining for Thbs1 (green) and nuclei (Hoechst 33342, magenta) in wounded skin on day 7 PWI. Dotted lines: approximate location of the basement membrane beneath the normal epidermis. Dotted lines: approximate location of the basement membrane beneath the leading edge or

Figure 6. *Continued*
neo-epidermis. Der, dermis; Epi, normal epidermis; Eschar, eschar; WEpi, neo-epidermis. Scale bars, 100 μm (low magnification), and 10 μm (high magnification).
(I) Quantification of the distance of Thbs1$^+$ keratinocytes to the neo-epidermis margin. Means of three to seven measurements at each time point are represented and bars represent the distance range.

Erk activity is indispensable for Thbs1$^+$ keratinocytes differentiation and epidermal wound healing *in vivo*

We next investigated the involvement of LPA in the epidermal wound healing process *in vivo*. We generated an epithelial debridement wound with a 6-mm punch in the dorsal skin and examined the effects of LPA on the healing of the epithelial wound. However, we could not detect any significant difference between LPA-treated and control groups (Figures S10A–S10C). We then examined the potential role of Erk activity in Thbs1$^+$ keratinocyte differentiation and wound healing using the MEK inhibitor, Trametinib (Yamaguchi et al., 2011), which could be administered orally *in vivo*. Mice were orally administered with vehicle or Trametinib at the dose of 1 mg/kg/day for 2 days before excisional wound induction on the dorsal skin (Figure 7A). We then collected the wounded skin on day 1 PWI and performed immunohistochemical staining for Thbs1. Consistently with our above results, we found that a large number of Thbs1$^+$ keratinocytes were induced in the basal layer of the epidermis near the wound edge in the control mice treated with vehicle (Figure 7B). On the other hand, only few Thbs1$^+$ keratinocytes were observed in the epidermal basal layer in mice treated with Trametinib (Figure 7C). Quantitative analysis further confirmed that the number of Thbs1$^+$ keratinocytes in the wounded epidermis was significantly reduced upon Trametinib treatment (Figure 7D). These results together suggest that the induction of Thbs1$^+$ keratinocytes upon wounding *in vivo* is dependent on Erk activity. Finally, we examined the effect of Trametinib on wound closure and reepithelialization. To this end, we conducted wound healing assay in vehicle-treated control mice and Trametinib-treated mice and monitored the wound closure rate on day 1, 2, 4, and 6 PWI. Trametinib treatment significantly delayed the wound closure throughout the repairing process (Figures 7E and 7F). Therefore, Erk activity is indispensable for Thbs1$^+$ keratinocyte differentiation and skin-wound healing *in vivo*.

DISCUSSION

Accumulating evidences have now unveiled a remarkable heterogeneity of keratinocytes in the skin (Joost et al., 2016, 2018, 2020; Cheng et al., 2018; Finnegan et al., 2019; Haensel et al., 2020; Reynolds et al., 2021). Such heterogeneity becomes even larger as skin is challenged by injury or inflammation (Joost et al., 2018; Cheng et al., 2018; Haensel et al., 2020; Reynolds et al., 2021). Our study employed scRNA-seq to investigate the differentiation of NHEKs and revealed a previously unsuspected THBS1$^+$ keratinocyte subpopulation that exhibits migration and wound-response signatures and does not belong to the conventional classification of keratinocyte subtypes in the epidermis. Importantly, we found that *THBS1*-expressing keratinocytes were rare in the control but LPA strongly promoted their differentiation *in vitro*. Given that LPA production through the catalytic activity of a keratinocyte-specific phospholipase A, mPA-PLA$_1\alpha$ (or LIPH), is known (Aoki et al., 2008; Diribarne et al., 2012), the small number of THBS1$^+$ keratinocytes observed in control conditions might be because of the effect of endogenous LPA produced by keratinocytes themselves in the culture. In this study, we also confirmed our previous report that LPA induces NHEK differentiation into FLG$^+$ granular keratinocytes (Sumitomo et al., 2019). Therefore, LPA has a potential to promote the differentiation of both THBS1$^+$ keratinocytes and FLG$^+$ granular keratinocytes *in vitro*.

The dual action of LPA on THBS1$^+$ keratinocyte differentiation and FLG$^+$ keratinocyte differentiation was mediated through LPA$_1$ and LPA$_5$ receptors and their downstream Rho/ROCK-SRF signaling. However, with the same LPA$_1$/LPA$_5$-RHO/ROCK-SRF axis responsible for both LPA-induced THBS1$^+$ and granular keratinocytes, then what determines the cell fate of NHEKs? Here, we showed that there was a heterogeneity of ERK activity in NHEKs before LPA stimulation. The heterogeneity of ERK activity in cells including keratinocytes was observed previously (Sampattavanich et al., 2018; Hiratsuka et al., 2015, 2020), and it was reported that changes in basal ERK activity and pulses account for different cell states and could dynamically regulate keratinocyte differentiation (Hiratsuka et al., 2020). Given that MEK inhibition specifically suppressed the differentiation of LPA-treated NHEKs into THBS1$^+$ keratinocytes, it is likely that THBS1$^+$ keratinocytes are derived from NHEK cells with high basal ERK activity. Moreover, as ERK activation can be propagated to neighboring cells via paracrine signaling (Aoki et al., 2013; Hiratsuka et al., 2020), this might also be involved in the cluster appearance of THBS1$^+$ keratinocytes that we observed *in vitro*. As

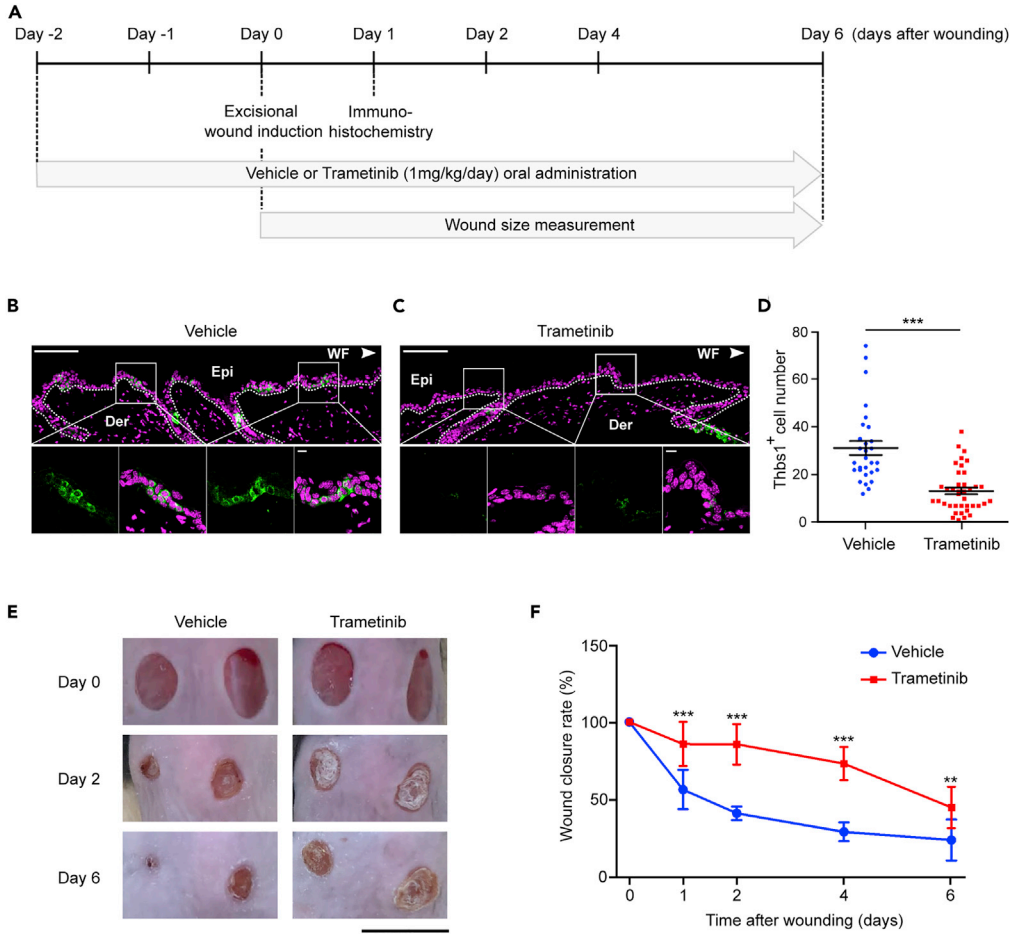

Figure 7. Erk inhibition suppressed wound-induced Thbs1$^+$ keratinocytes and impaired wound closure *in vivo*

(A) Scheme represents the experiment design. Mice were orally administered with either vehicle or Trametinib at a dose of 1 mg/kg per day.

(B and C) Representative stacked confocal images showing immunostaining for Thbs1 (green) and nuclei (Hoechst 33342, magenta) in wound skin of vehicle-treated mice (B) and Trametinib-treated mice (C) on day 1 PWI. The captured areas were within 1.5 mm distance from the wound front (WF). Dotted white lines indicate the approximate location of the basement membrane beneath the epidermis. Der, dermis; Epi, epidermis. Scale bars, 100 μm (low magnification), and 10 μm (high magnification).

(D) Quantification of the number of Thbs1$^+$ keratinocytes in the epidermis of vehicle-treated mice (left) and Trametinib-treated mice (right) on day 1 PWI. Thbs1$^+$ keratinocytes were counted within a range of 1.5 mm from the wound front. Multiple sections at different levels of four wounds from two mice were analyzed per each condition. Results are represented as means ± SEM, ***$p < 0.001$ (two-tailed Student's *t* test).

(E) Representative images on the same scale of wounds on dorsal skin of mice treated with either vehicle or Trametinib on day 0, 2, and six PWI. Scale bar, 1 cm.

(F) Quantification analysis of the wound closure rate on day 0, 1, 2, 4, and 6 PWI. The left and right wounds of four mice were monitored per each condition. Results are represented as means ± SD, **$p < 0.01$, ***$p < 0.001$ (two-tailed Student's *t* test comparing at each time point).

EGFR-specific inhibitor suppressed THBS1$^+$ keratinocyte differentiation in a similar fashion to suppression of ERK by MEK inhibitor, we suggest that a potential candidate for such paracrine signaling molecule is EGF. Notably, high ERK activity was observed in Ki67$^+$ proliferating keratinocytes that could be possibly driven by EGF. Therefore, it is likely that LPA acts on proliferating basal keratinocytes with high ERK activity and facilitates their differentiation into THBS1$^+$ keratinocytes.

It was previously reported that *Thbs1* expression is upregulated in the wound skin of mice (Joost et al., 2018; Haensel et al., 2020). Particularly, it was shown that *Thbs1* expression is upregulated in basal

keratinocytes upon skin wounding in the latter (Haensel et al., 2020). In this work, we have analyzed the publicly deposited scRNA-seq data of mouse normal skin and day 4 PWI wound skin in Haensel et al.'s paper (Haensel et al., 2020). We found that of basal keratinocytes, the GA basal keratinocytes expressed the highest level of *Thbs1* at this time point (Figure 5C) and were enriched in genes related to cell migration similarly to the *in vitro* human THBS1$^+$ keratinocytes, suggesting their migratory roles. Consistently, we found THBS1 is involved in keratinocyte migration as knockdown of *THBS1* impaired wound healing in *in vitro* scratching assay. It should be noted that not only THBS1-producing keratinocytes move faster but also the surrounding keratinocytes (Video S1). This might be possible because THBS1 is a secretory matrix protein that has a potential to remodel the microenvironment. *In vivo*, we demonstrated that Thbs1$^+$ keratinocytes were specifically and transiently induced in mouse skin upon wound injury by immunohistochemistry. These cells originate from basal keratinocytes in the proliferation zone distant from the wound edge (Aragona et al., 2017; Park et al., 2017). Thereafter, Thbs1$^+$ keratinocytes apparently detach from the basal layer, polarize, and migrate through the suprabasal layer toward the wound front and exit cell cycle (Figure S11). In wound healing, for the reepithelialization to take place efficiently, we speculate that these Thbs1$^+$ keratinocytes promote keratinocyte migration through the secretion of Thbs1. Consistently, delay of skin wound closure was reported in wounds treated with antisense-*Thbs1* (DiPietro et al., 1996) and in *Thbs1*-deficient mice (Agah et al., 2002; Nor et al., 2005). Eventually, upon Thbs1$^+$ keratinocytes' arrival at the wound, they differentiate into spinous keratinocytes and subsequently downregulate their Thbs1 expression (Figure S11). Therefore, we speculate that Thbs1$^+$ keratinocytes might also supply the keratinocytes for reepithelialization and stratification of the neo-epidermis in wound healing. However, given the small number of Thbs1$^+$ keratinocytes compared to the total keratinocytes in neo-epidermis after wounding, their contribution might be relatively small. In addition, it should be noted that *Thbs1* is also expressed by other cell types such as monocytes, macrophages, fibroblasts, and myofibroblasts. Because these cells could be observed in the injured dermis of wounded skin, it is possible that Thbs1 produced by these cells may also contribute to the wound healing besides Thbs1$^+$ keratinocytes in the epidermis.

Accumulating evidence has suggested different cellular states of IFE keratinocytes in wound healing; however, whether all wound-responsive IFE cells are derived from a single subpopulation is still an open question. Our study indicated that Thbs1$^+$ keratinocytes are differentiated from proliferating basal keratinocytes, then transiently migrate through the suprabasal layers toward the migratory zone before Thbs1 being downregulated as a consequence of terminal differentiation in the neo-epidermis. Given that IFE-derived keratinocytes were reported to make long-term contributions to the regenerative basal layer after migration (Plikus et al., 2012; Vagnozzi et al., 2015), it is possible that in addition to Thbs1$^+$ cells, other subpopulation(s) of IFE-derived keratinocytes are also involved in the wound healing process. In such a scenario, Thbs1$^+$ keratinocytes may account for early and fast reepithelialization actions, whereas other IFE keratinocyte subpopulation(s) are responsible for the subsequent permanent epidermal regeneration.

It is also known that in addition to IFE-derived cells, hair follicle (HF)-derived stem cells from the isthmus, junctional zone, and bulge also contribute to the neo-epidermis formation during the epidermal wound healing process (Plikus et al., 2012). It was reported that although the migration of HF-derived stem cells is relatively slower compared to that of IFE-derived cells, both are able to generate long-lasting clones in the regenerative epidermis together with transient suprabasal cells (Plikus et al., 2012; Vagnozzi et al., 2015). In this study, we also observed Thbs1$^+$ keratinocytes in hair follicles of normal skin. In addition, we were able to detect two subpopulations of HF keratinocytes that expressed high levels of *Thbs1* in Haensel et al.'s scRNA-seq data (Figures S12A–S12C). One is the *Lgr5*$^+$ HF stem cells that have been previously reported to migrate toward the wound front and contribute to the new-forming IFE epidermis (Joost et al., 2018). The other *Thbs1*-expressing HF subpopulation was enriched for intermediate early genes such as *Ier3*. However, it is not clear whether these cells could also migrate out of the bulge. This issue should be further addressed in future studies.

In this study, we also examined the effect of LPA on the differentiation of Thbs1$^+$ keratinocytes and skin wound healing in mice. However, we could not detect any obvious effect. There are several possible interpretations for this result. First, it is possible that Thbs1$^+$ keratinocytes *in vivo* are different from THBS1$^+$ keratinocytes that we have observed *in vitro*, and their differentiation is not dependent on LPA. Second, the response of keratinocytes to LPA might have already been saturated by the large amount of LPA released

upon skin wounding (Mazereeuw-Hautier et al., 2005). Third, other bioactive mediators might function redundantly to LPA *in vivo*. Finally, given that LPA is susceptible to oxidation and unstable *in vivo*, LPA might rapidly lose its activity in the *in vivo* experiment setting, thus making it difficult to be used as a therapeutic agent for wound healing. In such case, future development of LPA_1 and LPA_5 agonists that could be administered *in vivo* will help us to further clarify this issue.

Notably, in this work, we found that inhibition of Erk activity with a MEK inhibitor suppressed $Thbs1^+$ keratinocyte induction upon wounding *in vivo*. Therefore, Erk activity is also indispensable for $Thbs1^+$ keratinocytes both *in vitro* and *in vivo*. Moreover, we also found that MEK inhibitor suppressed wound healing. However, this result should be interpreted with caution. Given the pleiotropic biological role of MEK-ERK signaling, we could not exclude the possibility that MEK inhibitor may also interfere with other processes such as contraction that also contributes to wound healing in addition to the interference of $Thbs1^+$ keratinocyte differentiation. Nevertheless, our finding that wound healing is impaired upon MEK inhibitor treatment and the fact that various MEK inhibitors are now widely used in cancer therapy have implications for the treatment of these patients. It should also be noted that skin adverse effects are highly common in cancer patients who received MEK inhibitor treatment (Varvaresou et al., 2020).

Limitations of the study

Regarding the limitation of our study, firstly, it should be noted that *in vitro* maintenance of keratinocytes is not a physiological condition. Therefore, it is difficult to conclude that $THBS1^+$ keratinocytes we observed *in vitro* are exactly the same to those $Thbs1^+$ keratinocytes *in vivo*. However, given several similar characteristics between $THBS1^+$ keratinocytes *in vitro* and $Thbs1^+$ keratinocytes *in vivo* as discussed above, we suggest that it is possible to extract useful hypothesis from our *in vitro* studies for further validations. The second limitation of our study was although our suggestion for the migratory features of $THBS1^+$ keratinocytes during wound healing was based on a combination of *in vitro* assays, scRNA-seq data analysis, and spatiotemporal correlation of $Thbs1^+$ keratinocytes *in vivo*, the direct evidence is still lacking. The lineage tracing model would be an ideal approach to further confirm the nature of $THBS1^+$ keratinocytes in the future.

STAR★METHODS

Detailed methods are provided in the online version of this paper and include the following:

- KEY RESOURCES TABLE
- RESOURCE AVAILABILITY
  - Lead contact
  - Materials availability
  - Data and code availability
- EXPERIMENTAL MODEL AND SUBJECT DETAILS
  - Cell culture
  - Animal model
- METHOD DETAILS
  - Single-cell isolation, cDNA library preparation and next generation sequencing
  - Analysis of scRNA-seq data
  - scRNA-seq analysis of public data GEO: GSE142471
  - siRNA-mediated knockdown
  - Quantitative RT-PCR
  - NHEKs wound scratching assay
  - Time-lapse imaging
  - Immunocytochemistry
  - Immunohistochemistry
  - Wound healing experiments on mice
  - Topical application of LPA cream to the wounded skin
- QUANTIFICATION AND STATISTICAL ANALYSIS

SUPPLEMENTAL INFORMATION

Supplemental information can be found online at https://doi.org/10.1016/j.isci.2022.104130.

ACKNOWLEDGMENTS

We thank A. Fujimoto for advice on NGS data analysis, H. Shirakawa for advice on *in vivo* wound healing experiment, Y. Yoshii and A. Washio for technical assistance, and T. Arai for secretarial assistance. The supercomputing resource, "SHIROKANE," was provided by the Human Genome Center, The University of Tokyo (http://sc.hgc.jp/shirokane.html). This work was supported in part by Grants-in-Aid for Scientific Research from the Ministry of Education, Culture, Sports, Science, and Technology of Japan (grant number 17H01531 and to S.N. and grant number 20K07287 to D.T.); by a research grant from Ono Medical Research Foundation (grant number 203170600055 to D.T.); by a research grant from The Shimizu Foundation for Immunology and Neuroscience 2020 (D.T.) and by the Special Coordination Funds by the Ministry of Education, Culture, Sports, Science, and Technology of Japan and Astellas Pharma Inc. in Creation of Innovation Centers for Advanced Interdisciplinary Research Areas (S.N. and D.T.). S.N. and D.T. were supported by the Coordination Fund from JST and Astellas Pharma Inc.

AUTHOR CONTRIBUTIONS

R.S., A.Q.N., S.N., and D.T. designed the experiments. R.S. and D.T. performed single cell isolation, RNA extraction, and library preparation with the Fluidigm C1 system. S.S. conducted sequencing using the Illumina HiSeq2500. R.S., A.Q.N., and D.T. performed scRNA-seq data analysis. A.Q.N. and M.H. performed validation experiments with NHEKs. A.Q.N, D.T., and A.K. performed wound healing experiments with mice. A.Q.N. and D.T. conducted immunohistochemistry. A.Q.N., M.H., and D.T. performed statistical analysis. A.W. supervised scRNA-seq experiment and data analysis. R.S., A.Q.N., M.H., S.N., and D.T. wrote the manuscript. All authors reviewed and approved the manuscript.

DECLARATION OF INTERESTS

S.N. is a scientific advisor to Astellas Pharma Inc and Toray Co., Ltd. No potential conflicts of interest were disclosed by the other authors.

Received: April 15, 2021
Revised: October 19, 2021
Accepted: March 17, 2022
Published: April 15, 2022

REFERENCES

Abe, M., Sogabe, Y., Syuto, T., Yokoyama, Y., and Ishikawa, O. (2007). Evidence that PI3K, Rac, Rho, and Rho kinase are involved in basic fibroblast growth factor-stimulated fibroblast-collagen matrixcontraction. J. Cell. Biochem. *102*, 1290–1299.

Adams, J.C., and Lawler, J. (2011). The thrombospondins. Cold Spring Harb. Perspect. Biol. *3*, a009712.

Agah, A., Kyriakides, T.R., Lawler, J., and Bornstein, P. (2002). The lack of thrombospondin-1 (TSP1) dictates the course of wound healing in double-TSP1/TSP2-null mice. Am. J. Pathol. *161*, 831–839.

Aikawa, S., Hashimoto, T., Kano, K., and Aoki, J. (2015). Lysophosphatidic acid as a lipid mediator with multiple biological actions. J. Biochem. *157*, 81–89.

An, S., Bleu, T., Hallmark, O.G., and Goetzl, E.J. (1998). Characterization of a novel subtype of human G protein-coupled receptor for lysophosphatidic acid. J. Biol. Chem. *273*, 7906–7910.

Andrews, S. FastQC: A quality control tool for high throughput sequence data. http://www.bioinformatics.babraham.ac.uk/projects/fastqc.

Aoki, J., Inoue, A., and Okudaira, S. (2008). Two pathways for lysophosphatidic acid production. Biochim. Biophys. Acta *1781*, 513–518.

Aoki, K., Kumagai, Y., Sakurai, A., Komatsu, N., Fujita, Y., Shionyu, C., and Matsuda, M. (2013). Stochastic ERK activation induced by noise and cell-to-cell propagation regulates cell density-dependent proliferation. Mol. Cell *52*, 529–540.

Aragona, M., Dekoninck, S., Rulands, S., Lenglez, S., Mascré, G., Simons, B.D., and Blanpain, C. (2017). Defining stem cell dynamics and migration during wound healing in mouse skin epidermis. Nat. Commun. *8*, 14684.

Balazs, L., Okolicany, J., Ferrebee, M., Tolley, B., and Tigyi, G. (2001). Topical application of the phospholipid growth factor lysophosphatidic acid promotes wound healing in vivo. Am. J. Physiol. Regul. Integr. Comp. Physiol. *280*, R466-472.

Benitez, J.A., Cheng, S., and Deng, Q. (2017). Revealing allele-specific gene expression by single-cell transcriptomics. Int. J. Biochem. Cell Biol. *90*, 155–160.

Cañedo-Dorantes, L., and Cañedo-Ayala, M. (2019). Skin acute wound healing: a comprehensive review. Int. J. Inflam. *2019*, 3706315.

Cargnello, M., and Roux, P.P. (2011). Activation and function of the MAPKs and their substrates, the MAPK-activated protein kinases. Microbiol. Mol. Biol. Rev. *75*, 50–83.

Cheng, J.B., Sedgewick, A.J., Finnegan, A.I., Harirchian, P., Lee, J., Kwon, S., Fassett, M.S., Golovato, J., Gray, M., Ghadially, R., et al. (2018). Transcriptional programming of normal and inflamed human epidermis at single-cell resolution. Cell Rep. *25*, 871–883.

Cunha, D.A., Cito, M., Carlsson, P.O., Vanderwinden, J.M., Molkentin, J.D., Bugliani, M., Marchetti, P., Eizirik, D.L., and Cnop, M. (2016). Thrombospondin 1 protects pancreatic β-cells from lipotoxicity via the PERK-NRF2 pathway. Cell Death Differ. *23*, 1995–2006.

Demoyer, J.S., Skalak, T.C., and Durieux, M.E. (2000). Lysophosphatidic acid enhances healing of acute cutaneous wounds in the mouse. Wound Repair Regen. *8*, 530–537.

DiPietro, L.A., Nissen, N.N., Gamelli, R.L., Koch, A.E., Pyle, J.M., and Polverini, P.J. (1996). Thrombospondin 1 synthesis and function in wound repair. Am. J. Pathol. *148*, 1851–1860.

Diribarne, M., Mata, X., Riviere, J., Bouet, S., Vaiman, A., Chapuis, J., Reine, F., Fleurot, R., Auvinet, G., Deretz, S., et al. (2012). *LIPH*

expression in skin and hair follicles of normal coat and Rex rabbits. PLoS One *7*, e30073.

Dobin, A., Davis, C.A., Schlesinger, F., Drenkow, J., Zaleski, C., Jha, S., Batut, P., Chaisson, M., and Gingeras, T.R. (2013). STAR: ultrafast universal RNA-seq aligner. Bioinformatics *29*, 15–21.

Elias, P.M. (2007). The skin barrier as an innate immune element. Semin. Immunopathol. *29*, 3–14.

Finnegan, A., Cho, R.J., Luu, A., Harirchian, P., Lee, J., Cheng, J.B., and Song, J.S. (2019). Single-cell transcriptomics reveals spatial and temporal turnover of keratinocyte differentiation regulators. Front. Genet. *10*, 775.

Fitsialos, G., Chassot, A.A., Turchi, L., Dayem, M.A., LeBrigand, K., Moreilhon, C., Meneguzzi, G., Buscà, R., Mari, B., Barbry, P., et al. (2007). Transcriptional signature of epidermal keratinocytes subjected to in vitro scratch wounding reveals selective roles for ERK1/2, p38, and phosphatidylinositol 3-kinase signaling pathways. J. Biol. Chem. *282*, 15090–15102.

Gribov, A., Sill, M., Lück, S., Rücker, F., Döhner, K., Bullinger, L., Benner, A., and Unwin, A. (2010). SEURAT: visual analytics for the integrated analysis of microarray data. BMC Med. Genomics *3*, 21.

Grün, D., Lyubimova, A., Kester, L., Wiebrands, K., Basak, O., Sasaki, N., Clevers, H., and Oudenaarden, A.V. (2015). Single-cell messenger RNA sequencing reveals rare intestinal cell types. Nature *525*, 251–255.

Haensel, D., Jin, S., Sun, P., Cinco, R., Dragan, M., Nguyen, Q., Cang, Z., Gong, Y., Vu, R., MacLean, A.L., et al. (2020). Defining epidermal basal cell states during skin homeostasis and wound healing using single-cell transcriptomics. Cell Rep. *30*, 3932–3947.

Hayashi, K., Watanabe, B., Nakagawa, Y., Minami, S., and Morita, T. (2014). RPEL proteins are the molecular targets for CCG-1423, an inhibitor of Rho signaling. PLoS One *9*, e89016.

Hiratsuka, T., Bordeu, I., Pruessner, G., and Watt, F.M. (2020). Regulation of ERK basal and pulsatile activity control proliferation and exit from the stem cell compartment in mammalian epidermis. Proc. Natl. Acad. Sci. U S A *117*, 17796–17807.

Hiratsuka, T., Fujita, Y., Naoki, H., Aoki, K., Kamioka, Y., and Matsuda, M. (2015). Intercellular propagation of extracellular signal-regulated kinase activation revealed by in vivo imaging of mouse skin. Elife *4*, e05178.

Inoue, A., Arima, N., Ishiguro, J., Prestwich, G.D., Arai, H., and Aoki, J. (2011). LPA-producing enzyme PA-PLA$_1\alpha$ regulates hair follicle development by modulating EGFR signalling. EMBO J. *30*, 4248–4260.

Jerónimo, A., Rodrigues, G., Vilas-Boas, F., Martins, G.G., Bagulho, A., and Real, C. (2017). Hydrogen peroxide regulates angiogenesis-related factors in tumor cells. Biochem. Cell Biol. *95*, 679–685.

Joost, S., Annusver, K., Jacob, T., Sun, X., Dalessandri, T., Sivan, U., Sequeira, I., Sandberg, R., and Kasper, M. (2020). The molecular anatomy of mouse skin during hair growth and rest. Cell Stem Cell *26*, 441–457.

Joost, S., Jacob, T., Sun, X., Annusver, K., Manno, G.L., Sur, I., and Kasper, M. (2018). Single-cell transcriptomics of traced epidermal and hair follicle stem cells reveals rapid adaptations during wound healing. Cell Rep *25*, 585–597.

Joost, S., Zeisel, A., Jacob, T., Sun, X., Manno, G.L., Lönnerberg, P., Linnarsson, S., and Kasper, M. (2016). Single-cell transcriptomics reveals that differentiation and spatial signatures shape epidermal and hair follicle heterogeneity. Cell Syst. *3*, 221–237.

Kim, D.S., Kim, S.Y., Kleuser, B., Schäfer-Korting, M., Kim, K.H., and Park, K.C. (2004). Sphingosine-1-phosphate inhibits human keratinocyte proliferation via Akt/protein kinase B inactivation. Cell. Signal. *16*, 89–95.

Kolodziejczyk, A.A., Kim, J.K., Svensson, V., Marioni, J.C., and Teichmann, S.A. (2015). The technology and biology of single-cell RNA sequencing. Mol. Cell *58*, 610–620.

Korsunsky, I., Millard, N., Fan, J., Slowikowski, K., Zhang, F., Wei, K., Baglaenko, Y., Brenner, M., Loh, P., and Raychaudhuri, S. (2019). Fast, sensitive, and accurate integration of single cell data with Harmony. Nat. Methods *16*, 1289–1296.

Lemmon, M.A., and Schlessinger, J. (2010). Cell signaling by receptor tyrosine kinases. Cell *141*, 1117–1134.

Liao, Y., Smyth, G.K., and Shi, W. (2014). featureCounts: an efficient general purpose program for assigning sequence reads to genomic features. Bioinformatics *30*, 923–930.

Martin, M. (2011). Cudadapt removes adapter sequences from high-throughput sequencing reads. EMBnet J. *17*, 10–12.

Mazereeuw-Hautier, J., Gres, S., Fanguin, M., Cariven, C., Fauvel, J., Perret, B., Chap, H., Salles, J.P., and Saulnier-Blache, J.S. (2005). Production of lysophosphatidic acid in blister fluid: involvement of a lysophospholipase D activity. J. Invest. Dermatol. *125*, 421–427.

McGrath, J.A., Eady, R.A.J., and Pope, F.M. (2004). Anatomy and organization of human skin. In Rook's Textbook of Dermatology, T. Burns, S. Breathnach, N. Cox, and C. Griffiths, eds. (Blackwell Science Ltd Oxford), pp. 3.1–3.84.

Mio, T., Liu, X., Toews, M.L., and Rennard, S.I. (2002). Lysophosphatidic acid augments fibroblast-mediated contraction of released collagen gels. J. Lab. Clin. Med. *139*, 20–27.

Nor, J.E., Dipietro, L., Murphy-Ullrich, J.E., Hynes, R.O., Lawler, J., and Polverini, P.J. (2005). Activation of latent TGF-β1 by thrombospondin-1 is a major component of wound repair. Oral Biosci. Med. *2*, 153–161.

Park, S., Gonzalez, D.G., Guirao, B., Boucher, J.D., Cockburn, K., Marsh, E.D., Mesa, K.R., Brown, S., Rompolas, P., Haberman, A.M., et al. (2017). Tissue-scale coordination of cellular behaviour promotes epidermal wound repair in live mice. Nat. Cell Biol. *19*, 155–163.

Pasternack, S.M., Kügelgen, I.V., Aboud, K.A., Lee, Y.A., Rüschendorf, F., Voss, K., Hillmer, A.M., Molderings, G.J., Franz, T., Ramirez, A., et al. (2008). G protein-coupled receptor P2Y5 and its ligand LPA are involved in maintenance of human hair growth. Nat. Genet. *40*, 329–334.

Plikus, M.V., Gay, D.L., Treffeisen, E., Wang, A., Supapannachart, R.J., and Cotsarelis, G. (2012). Epithelial stem cells and implications for wound repair. Semin. Cell Dev. Biol. *23*, 946–953.

Resovi, A., Pinessi, D., Chiorino, G., and Taraboletti, G. (2014). Current understanding of the thrombospondin-1 interactome. Matrix Biol. *37*, 83–91.

Reynolds, G., Vegh, P., Fletcher, J., Poyner, E.F.M., Stephenson, E., Goh, I., Botting, R.A., Huang, N., Olabi, B., Dubois, A., et al. (2021). Developmental cell programs are co-opted in inflammatory skin disease. Science *371*, eaba6500.

Rizvi, A.H., Camara, P.G., Kandror, E.K., Roberts, T.J., Schieren, I., Maniatis, T., and Rabadan, R. (2017). Single-cell topological RNA-seq analysis reveals insights into cellular differentiation and development. Nat. Biotechnol. *35*, 551–560.

Sampattavanich, S., Steiert, B., Kramer, B.A., Gyori, B.M., Albeck, J.G., and Sorger, P.K. (2018). Encoding growth factor identity in the temporal dynamics of FOXO3 under the combinatorial control of ERK and AKT kinases. Cell Syst. *6*, 664–678.

Shimomura, Y., Wajid, M., Ishii, Y., Shapiro, L., Petukhova, L., Gordon, D., and Christiano, A.M. (2008). Disruption of P2RY5, an orphan G protein-coupled receptor, underlies autosomal recessive woolly hair. Nat. Genet. *40*, 335–339.

Streit, M., Velasco, P., Riccardi, L., Spencer, L., Brown, L.F., Janes, L., Lange-Asschenfeldt, B., Yano, K., Hawighorst, T., Iruela-Arispe, L., et al. (2000). Thrombospondin-1 suppresses wound healing and granulation tissue formation in the skin of transgenic mice. EMBO J. *19*, 3272–3282.

Subramanian, A., Tamayo, P., Mootha, V.K., Mukherjee, S., Ebert, B.L., Gillette, M.A., Paulovich, A., Pomeroy, S.L., Golub, T.R., Lander, E.S., and Mesirov, J.P. (2005). Gene set enrichment analysis: a knowledge-based approach for interpreting genome-wide expression profiles. Proc. Natl. Acad. Sci. U S A *102*, 15545–15550.

Sumitomo, A., Siriwach, R., Thumkeo, D., Ito, K., Nakagawa, R., Tanaka, N., Tanabe, K., Watanabe, A., Kishibe, M., Ishida-Yamamoto, A., et al. (2019). LPA induces keratinocyte differentiation and promotes skin barrier function through the LPAR1/LPAR5-RHO-ROCK-SRF axis. J. Invest. Derm. *139*, 1010–1022.

Sweetwyne, M.T., and Murphy-Ullrich, J.E. (2012). Thrombospondin1 in tissue repair and fibrosis: TGF-β-dependent and independent mechanisms. Matrix Biol. *31*, 178–186.

Tan, K., and Lawler, J. (2009). The interaction of Thrombospondins with extracellular matrix proteins. J. Cell Commun. Signal. *3*, 177–187.

Tang, F., Barbacioru, C., Wang, Y., Nordman, E., Lee, C., Xu, N., Wang, X., Bodeau, J., Tuch, B.B., Siddiqui, A., et al. (2009). mRNA-Seq whole-transcriptome analysis of a single cell. Nat. Methods *6*, 377–382.

Uehata, M., Ishizaki, T., Satoh, H., Ono, T., Kawahara, T., Morishita, T., Tamakawa, H., Yamagami, K., Inui, J., Maekawa, M., et al. (1997). Calcium sensitization of smooth muscle mediated by a Rho-associated protein kinase in hypertension. Nature *389*, 990–994.

Vagnozzi, A.N., Reiter, J.F., and Wong, S.Y. (2015). Hair follicle and interfollicular epidermal stem cells make varying contributions to wound regeneration. Cell Cycle *14*, 3408–3417.

Varvaresou, A., Iakovou, K., Mellou, F., Myrogiannis, D., and Papageorgiou, S. (2020). Targeted therapy in oncology patients and skin: pharmaceutical and dermocosmetic management. J. Cosmet. Dermatol. *19*, 782–788.

Wu, T., Hu, E., Xu, S., Chen, M., Guo, P., Dai, Z., Feng, T., Zhou, L., Tang, W., Zhan, L., et al. (2021). clusterProfiler 4.0: a universal enrichment tool for interpreting omics data. Innov. J. *2*, 100141.

Xue, Z., Huang, K., Cai, C., Cai, L., Jiang, C.Y., Feng, Y., Liu, Z., Zeng, Q., Cheng, L., Sun, Y.E., et al. (2013). Genetic programs in human and mouse early embryos revealed by single-cell RNA sequencing. Nature *500*, 593–597.

Yamaguchi, T., Kakefuda, R., Tajima, N., Sowa, Y., and Sakai, T. (2011). Antitumor activities of JTP-74057 (GSK1120212), a novel MEK1/2 inhibitor, on colorectal cancer cell lines in vitro and in vivo. Int. J. Oncol. *39*, 23–31.

Yu, G., Wang, L.G., Han, Y., and He, Q.Y. (2012). clusterProfiler: an R package for comparing biological themes among gene clusters. OMICS J. Integr. Biol. *16*, 284–287.

Yung, Y.C., Stoddard, N.C., Mirendil, H., and Chun, J. (2015). Lysophosphatidic acid signaling in the nervous system. Neuron *85*, 669–682.

Zhao, Y., Shimizu, T., Nishihira, J., Koyama, Y., Kushibiki, T., Honda, A., Watanabe, H., Abe, R., Tabata, Y., and Shimizu, H. (2005). Tissue regeneration using macrophage migration inhibitory factor-impregnated gelatin microbeads in cutaneous wounds. Am. J. Pathol. *167*, 1519–1529.

STAR★METHODS

KEY RESOURCES TABLE

REAGENT or RESOURCE	SOURCE	IDENTIFIER
Antibodies		
Mouse monoclonal anti-THBS1	Invitrogen	Cat# MA5-13398; RRID: AB_10984611
Mouse monoclonal anti-THBS1	Santa Cruz	Cat# sc-59887; RRID: AB_793045
Rabbit polyclonal anti-THBS1	Abcam	Cat# ab85762; RRID: AB_10674322
Mouse monoclonal anti-FLG	Santa Cruz	Cat# sc-66192; RRID: AB_1122916
Rabbit polyclonal anti-Krt10	Biolegend	Cat# PRB-159P; RRID: AB_291580
Mouse monoclonal anti-KRT14 (Alexa Fluor 647-conjugated)	Santa Cruz	Cat# sc53253; RRID: AB_2134820
Mouse monoclonal anti-Ki67	Leica	Cat# NCL-L-Ki67-MM1; RRID: AB_563841
Rabbit monoclonal anti-Ki67	Sigma	Cat# ZRB1007
Mouse monoclonal anti-MAP kinase, Activated (phosphorylated)	Sigma	Cat# M8159; RRID: AB_477245
Chemicals, peptides, and recombinant proteins		
Recombinant human IL-4	PeproTech	Cat# 200-04
LPA 18:1	Avanti Polar Lipids	Cat# 287130
AM095	Sigma	Cat# BM0029
TCLPA54	Tocris	Cat# 4708/10
Y-27632	Wako	Cat# 259-00613
U0126	Sigma	Cat# 19-147
CCG-1423	Sigma	Cat# 555558
PD168393	Sigma	Cat# 194423-15-9
Wortmannin	Tocris	Cat# 1232/1
Trametinib	ChemScene	Cat# CS-0060
Lipofectamine RNAiMAX Transfection Reagent	Life Technologies	Cat# 13778150
Critical commercial assays		
C1 Single-Cell Open App IFC, 17 - 25 µm	Fluidigm	Cat# 100-8135
Click-iT™ TUNEL Alexa Fluor™ 488 Imaging Assay	Thermo Fisher	Cat# C10245
Deposited data		
scRNA-seq data	This paper	GEO: GSE167056
Raw quantification data	This paper	Mendeley Data: https://doi.org/10.17632/693s5mbxnn.1
Experimental models: Cell lines		
Normal Human Epidermal Keratinocytes (NHEKs)	KURABO	Cat# KK-4009
Experimental Models: Organisms/Strains		
C57BL/6N	SLC	N/A
Oligonucleotides		
Primers for qPCR	This paper	N/A
Silencer Select siRNAs	Life Technologies	N/A

(*Continued on next page*)

Continued

REAGENT or RESOURCE	SOURCE	IDENTIFIER
Software and algorithms		
FastQC v0.11.8	Andrews, 2010	https://github.com/s-andrews/FastQC
Cutadapt v2.3	Martin, 2011	https://github.com/marcelm/cutadapt
STAR v2.7.0f	Dobin et al., 2013	https://github.com/alexdobin/STAR
featureCounts v1.6.4	Liao et al., 2014	http://bioinf.wehi.edu.au/featureCounts/
Seurat v3.1.5	Gribov et al., 2010	https://github.com/satijalab/seurat
Harmony v1.0	Korsunsky et al., 2019	https://github.com/pardeike/Harmony
GSEA	Subramanian et al., 2005	https://www.gsea-msigdb.org/gsea/index.jsp
clusterProfiler	Yu et al., 2012; Wu et al., 2021	https://github.com/YuLab-SMU/clusterProfiler
Prism	Graphpad	https://www.graphpad.com/scientific-software/prism/
ImageJ	NIH	https://imagej.nih.gov/ij/
Imaris	Oxford Instruments	N/A

RESOURCE AVAILABILITY

Lead contact

Requests for resources and reagents should be directed to and will be fulfilled by the lead contact, Dean Thumkeo (d.thumkeo@mfour.med.kyoto-u.ac.jp).

Materials availability

This study did not generate new unique reagents.

Data and code availability

The scRNA-seq data were deposited in Gene Expression Omnibus (GEO) repository, NCBI (GEO: GSE167056). All codes used were from prior reports, as listed in the "Software and Algorithms" section of the key resources table. Raw quantification data have been deposited at Mendeley (Mendeley Data: https://doi.org/10.17632/693s5mbxnn.1) and are public available as the data of publication. Any additional information required to reanalyze the data reported in this paper is available from the lead contact upon request.

EXPERIMENTAL MODEL AND SUBJECT DETAILS

Cell culture

Normal Human Epidermal Keratinocytes (NHEKs, KURABO) were used at passages 1-2 and maintained in an undifferentiated state in HuMedia KG-2 media (KURABO). At 24 h after seeding, cells were starved in EpiLife medium (Invitrogen) containing 60 μM Ca^{2+} (Gibco) in the absence of growth factors for 48 h. For stimulation, cells were cultured in EpiLife medium containing 1.2 mM Ca^{2+} (Gibco) and supplemented with 30 ng/ml recombinant human IL-4 in the presence or absence of LPA. Depending on the assay, cells were pretreated with either AM095 (10 μM), TCLPA54 (3 μM), Y-27632 (30 μM), CCG-1423 (3 μM), U0126 (5 μM or 10 μM), PD168393 (1 μM), or Wortmannin (1 μM) prior to stimulation.

Animal model

C57BL/6N mice (female, 6-7 week old) were purchased from SLC (Shizuoka, Japan) and kept under pathogen-free conditions. All animal experiments were conducted in accordance with the US National Institutes of Health Guide for the Care and Use of Laboratory Animals and approved by the Institutional Animal Care and Use Committee of Kyoto University Graduate School of Medicine.

METHOD DETAILS

Single-cell isolation, cDNA library preparation and next generation sequencing

At 72 h post stimulation, single cell suspension of 300 cells/μl from either vehicle control or LPA stimulation was prepared and loaded into a 96-well microfluidic chip (designed for cells from 17 - 25 μm diameter) for single cell capture using the Fluidigm C1 Autoprep system. The capturing efficiency was evaluated on a

microscope and only single cells were subjected to library preparation. The SMART-Seq® v4 (Clontech) was used for cDNA synthesis from the single cells. Library was amplified using the Nextera XT DNA Library Preparation Kit (Illumina) and quality control on multiplexed libraries was performed by Bioanalyzer 2100 (Agilent). Finally, libraries were deep sequenced as single-ended on an Illumina HiSeq 2500 platform.

Analysis of scRNA-seq data

Raw sequencing data in FASTQ format was evaluated using FastQC (v0.11.8) and adapter sequences were removed with Cutadapt (v2.3, Martin, 2011). Then reads were mapped to the reference genome (hg38) together with the GENCODE v30 annotation file using STAR (v2.7.0f, Dobin et al., 2013). A count matrix was generated with featureCounts (v1.6.4, Liao et al., 2014) for downstream analysis in R (v3.6.3).

Cells with total counts of less than 500,000, total number of expressed genes less than 2,000, a percentage of counts in mitochondrial genes more than 30%, and genes expressed in less than 2 cells were excluded. Raw counts were normalized by library size and log-transformed with *NormalizeData* function in Seurat R package (v3.1.5, Gribov et al., 2010). We performed batch correction by applying Harmony (v1.0, Korsunsky et al., 2019) onto the principle component analysis (PCA) matrix with theta = 0.5. The batch corrected PCA matrix was then used for clustering and UMAP visualization with Seurat. DEG analysis was performed based on two-sided Wilcoxon rank sum test using the default Seurat's function *FindAllMarkers*. GO analysis was conducted using TPM values with GSEA tools (Subramanian et al., 2005) on GO gene sets.

scRNA-seq analysis of public data GEO: GSE142471

Haensel et al.'s scRNA-seq data (GEO: GSE142471) was downloaded from the GEO repository. Count matrices were imported and similar quality control parameters were used to filter cells with 200 - 5,000 genes and less than 10% mitochondrial percentage as previously described by Haensel et al. Two unwounded and three wounded skin samples were integrated together and downstream analysis was similarly performed as described above in "analysis for scRNA-seq data" using Seurat and Harmony.

siRNA-mediated knockdown

NHEKs were transfected with Silencer Select siRNAs (at a final concentration of 5 nM) using Lipofectamine RNAiMAX (Life Technologies) at 36 h prior to stimulation. Silencer Select Negative control no. 1 (Life Technologies) was used as a negative control in all experiments. The sequences of Silencer Select siRNAs used were as follows:

LPAR1: GAGACUGACUGUUAGCACAtt and

UGUGCUAACAGUCAGUCUCcg,

LPAR5: AGUGACUUGUGACAAUUUAtt and

UAAAUUGUCACAAGUCACUat,

THBS1: GGACUGCGUUGGUGAUGUAtt and

UACAUCACCAACGCAGUCCtt.

Quantitative RT-PCR

mRNA was extracted from cells using TRIzol® LS Reagent (Life Technologies) and reverse-transcribed to cDNA using PrimeScript RT Master Mix (TaKaRa). cDNA, primers, and TB Green Premix Ex Taq (Tli RNaseH Plus) (TaKaRa) were mixed in a 96-well PCR plate. Subsequently, quantitative PCR (qPCR) was performed using a CFX96 Real-Time System (Bio-Rad). The sequences of primers are as the following:

FLG F: 5′-AGTCACGTGGCAGTCCTCACA-3′,

FLG R: 5′-TCTAAACCCGGATTCACCATAATCA-3′,

GAPDH F: 5′-ATGACATCAAGAAGGTGGTG-3′,

GAPDH R: 5′-CATACCAGGAAATGAGCTTG-3′,

LPAR1 F: 5′-AATCGGGATACCATGATGAGTCTT-3′,

LPAR1 R: 5′-CCAAGGAGTCCAGCAGATGATAAA-3′,

LPAR5 F: 5′-CGCCATCTTCCAGATGAAC-3′

LPAR5 R: 5′-TAGCGGTCCACGTTGATG-3′,

THBS1 F: 5′-GCTGGAAATGTGGTGCTTGTCC -3′,

THBS1 R: 5′-CTCCATTGTGGTTGAAGCAGGC-3′.

NHEKs wound scratching assay

The cell scratching was conducted using the P200 pipette tip. NHEKs at the confluency 70-80% were scratched to generate a wound with the width ~300 - 400 μm. Cell stimulation was conducted by the addition of 1.2 mM Ca^{2+} or of 10 μM LPA plus 1.2 mM Ca^{2+} immediately after wound scratching.

Time-lapse imaging

Time-lapse imaging of NHEKs wound healing *in vitro* was performed using BZ-X700 microscope (Keyence, Japan) equipped with a 10x dry objective lens (Keyence, Japan) and a chamber box to stably control the temperature (37°C) and CO_2 level (5%). Phase-contrast images were acquired every 5 min for 10 h.

Immunocytochemistry

Cultured cells were washed with phosphate-buffered saline (PBS), fixed in 4% paraformaldehyde (PFA) in PBS, permeabilized and blocked in PBS containing 10% normal goat/donkey serum and 0.3% Triton X-100. Cells were incubated with primary antibodies for FLG (1:200), THBS1 (1:500 (Abcam, ab85762) or 1:250 (Invitrogen, MA5-13398)), MAP kinase, activated (1:50), or Ki67 (1:500) overnight at 4°C and counter-stained with Hoechst 33342 (1:1000). Fluorescence images were acquired with an LSM 710 confocal microscope (Zeiss) using a 40x NA 1.30 oil-immersion objective lens or a FV3000 confocal microscope (Olympus) using a 20x NA 0.8 objective lens, 40x NA 0.95 objective lens or 60x NA 1.42 oil-immersion objective lens. Images were processed by Imaris software (Bitplane) and ImageJ (NIH).

Immunohistochemistry

Normal skin and wounded skin samples at different days after wounding were collected and fixed in 4% PFA overnight, cryoprotected in PBS containing 30% sucrose, frozen in Tissue-Tek OCT compound (Sakura), and cut into sections of 5 μm thickness using a cryostat (Leica). Antigen retrieval was performed in 10 mM citrate buffer (pH 5.8) using a pressure cooker. Sections were incubated with primary antibodies for either THBS1 (1:500 (Abcam, ab85762) or 1:250 (Santa Cruz, sc-59887)), Krt10 (1:2000), KRT14 (1:500) or Ki67 (1:500) overnight at 4°C and counterstained with Hoechst 33342 (1:1000). Fluorescence images were acquired with a TCS SP8 scanning confocal microscope (Leica) using a 40x NA 1.30 oil-immersion objective lens or FV3000 confocal microscope (Olympus) using a 20x NA objective lens. Images were processed by Imaris software (Bitplane) and ImageJ (NIH).

Wound healing experiments on mice

Mice received oral administration of vehicle or Trametinib prior to wound induction. Trametinib dissolved in 10% PEG400 (Nacalai) and 10% Cremophor EL (Nacalai) in sterile dH_2O was administered as a single dose of 1mg/kg per day. For immunohistochemistry experiments, four 3 mm full thickness wounds were created by ear punch on the dorsal telogen phase skin of each anesthetized mouse. For wound closure monitoring experiment, 8 mm biopsy punch (KAI Medical) was used to generate 2 wounds on the dorsal telogen phase skin of each anesthetized mouse.

Topical application of LPA cream to the wounded skin

Due to the hydrophobic nature of LPA, 1% LPA cream for topical application was prepared by adding 18:1 LPA into the following ingredients (constituent concentration, wt.%): milliQ water 56, propylene glycol (Nacalai) 10, paraffin liquid 10, vaseline (Nacalai) 5, glycerol monostearate (Alfa aesar) 10, 1-hexadecanol

(Nacalai) 6, polyoxyethylene hexadecyl ether (Nacalai) 2. Control vehicle cream formulation was the same as above except that milliQ water was 57 (constituent concentration, wt.%). Lipid phase and water phase were separately heated to 70°C, then combined and homogenized by T10 basic ULTRA-TURRAX Homogenizer (IKA) and cooled down. LPA was added before cooling down to room temperature. Control vehicle cream (25 mg) or 1% LPA cream (25 mg) was topically applied to the wounded skin for consecutive 4 days, twice for the first 2 days and once thereafter.

QUANTIFICATION AND STATISTICAL ANALYSIS

Prism (GraphPad Software) was used for statistical analyses. Data were presented as means ± standard deviation (SD) or means ± standard error of the mean (SEM). When only two groups were compared, a two-tailed Student's t-test was used. Alternatively, multiple comparisons were performed using one-way ANOVA followed by Bonferroni's post-hoc comparisons test for parametric data and the Kruskal-Wallis test followed by Dunn's multiple comparisons test for non-parametric data.